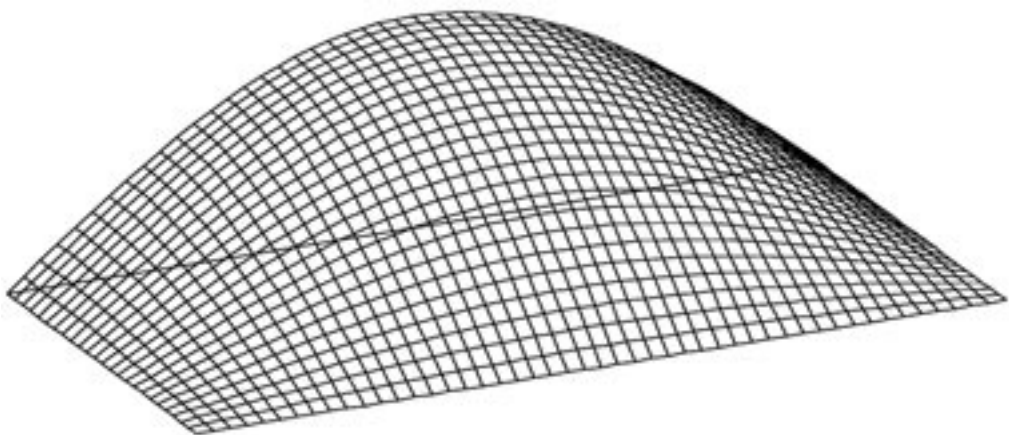


Thermal Buckling Analysis of Rectangular Panels Subjected to Humped Temperature Profile Heating

*William L. Ko
NASA Dryden Flight Research Center
Edwards, California*



The NASA STI Program Office...in Profile

Since its founding, NASA has been dedicated to the advancement of aeronautics and space science. The NASA Scientific and Technical Information (STI) Program Office plays a key part in helping NASA maintain this important role.

The NASA STI Program Office is operated by Langley Research Center, the lead center for NASA's scientific and technical information. The NASA STI Program Office provides access to the NASA STI Database, the largest collection of aeronautical and space science STI in the world. The Program Office is also NASA's institutional mechanism for disseminating the results of its research and development activities. These results are published by NASA in the NASA STI Report Series, which includes the following report types:

- **TECHNICAL PUBLICATION.** Reports of completed research or a major significant phase of research that present the results of NASA programs and include extensive data or theoretical analysis. Includes compilations of significant scientific and technical data and information deemed to be of continuing reference value. NASA's counterpart of peer-reviewed formal professional papers but has less stringent limitations on manuscript length and extent of graphic presentations.
- **TECHNICAL MEMORANDUM.** Scientific and technical findings that are preliminary or of specialized interest, e.g., quick release reports, working papers, and bibliographies that contain minimal annotation. Does not contain extensive analysis.
- **CONTRACTOR REPORT.** Scientific and technical findings by NASA-sponsored contractors and grantees.

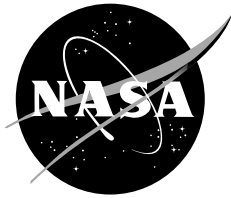
- **CONFERENCE PUBLICATION.** Collected papers from scientific and technical conferences, symposia, seminars, or other meetings sponsored or cosponsored by NASA.
- **SPECIAL PUBLICATION.** Scientific, technical, or historical information from NASA programs, projects, and mission, often concerned with subjects having substantial public interest.
- **TECHNICAL TRANSLATION.** English-language translations of foreign scientific and technical material pertinent to NASA's mission.

Specialized services that complement the STI Program Office's diverse offerings include creating custom thesauri, building customized databases, organizing and publishing research results...even providing videos.

For more information about the NASA STI Program Office, see the following:

- Access the NASA STI Program Home Page at <http://www.sti.nasa.gov>
- E-mail your question via the Internet to help@sti.nasa.gov
- Fax your question to the NASA Access Help Desk at (301) 621-0134
- Telephone the NASA Access Help Desk at (301) 621-0390
- Write to:
NASA Access Help Desk
NASA Center for AeroSpace Information
7121 Standard Drive
Hanover, MD 21076-1320

NASA/TP-2004-212041



Thermal Buckling Analysis of Rectangular Panels Subjected to Humped Temperature Profile Heating

*William L. Ko
NASA Dryden Flight Research Center
Edwards, California*

National Aeronautics and
Space Administration

Dryden Flight Research Center
Edwards, California 93523-0273

January 2004

NOTICE

Use of trade names or names of manufacturers in this document does not constitute an official endorsement of such products or manufacturers, either expressed or implied, by the National Aeronautics and Space Administration.

Available from the following:

NASA Center for AeroSpace Information (CASI)
7121 Standard Drive
Hanover, MD 21076-1320
(301) 621-0390

National Technical Information Service (NTIS)
5285 Port Royal Road
Springfield, VA 22161-2171
(703) 487-4650

CONTENTS

	<u>Page</u>
ABSTRACT	1
NOMENCLATURE	1
Acronyms	1
Symbols	1
INTRODUCTION	3
HUMPED TEMPERATURE PROFILES	4
Dome-Shaped Temperature Profile	4
Roof-Shaped Temperature Profile	4
PROBLEMS INVESTIGATED	5
FINITE-ELEMENT BUCKLING ANALYSIS	5
Panel Geometry	5
Material Properties	5
Boundary Conditions	6
Thermal Loads	6
BUCKLING TEMPERATURE MAGNIFICATION FACTORS	7
MINIMUM POTENTIAL ENERGY BUCKLING ANALYSIS	8
Energy Equations	8
Deformation Functions	9
Buckling Equations	9
Buckling Temperatures for Isotropic Cases	11
RESULTS	13
Buckling Temperature Magnification Factors	13
In-Plane Deformations	18
Thermal Stresses	18
CONCLUDING REMARKS	19
APPENDIX A—TEMPERATURE-DEPENDENT MATERIAL PROPERTIES OF HAYNES 230 ALLOY	21
APPENDIX B—COEFFICIENTS OF CHARACTERISTIC EQUATIONS	22
APPENDIX C—TABLE OF SPECIAL INTEGRALS	27
APPENDIX D—BUCKLING EQUATIONS	29
REFERENCES	33
FIGURES	34

ABSTRACT

This research investigates thermal buckling characteristics of rectangular panels subjected to different types of humped temperature profile heating. Minimum potential energy and finite-element methods are used to calculate the panel buckling temperatures. The two methods give fairly close thermal buckling solutions. “Buckling temperature magnification factor of the first kind, η ” is established for the fixed panel edges to scale up the buckling solution of uniform temperature loading case to give the buckling solution of the humped temperature profile loading cases. Also, “buckling temperature magnification factor of the second kind, ξ ” is established for the free panel edges to scale up the buckling solution of humped temperature profile loading cases with unheated boundary heat sinks to give the buckling solutions when the boundary heat sinks are heated up.

NOMENCLATURE

Acronyms

BC	boundary condition
JLOC	joint location
SPAR	Structural Performance and Resizing
TPS	thermal protection system

Symbols

A_{kl} Fourier coefficient of trial function for out-of-plane displacement w , in.

\bar{A}_{ij} extensional stiffness of orthotropic plates, $\bar{A}_{11} = \frac{t_s E_x}{1 - \nu_{xy} \nu_{yx}}$, $\bar{A}_{12} = \frac{t_s \nu_{yx} E_x}{1 - \nu_{xy} \nu_{yx}}$,
 $\bar{A}_{21} = \frac{t_s \nu_{xy} E_y}{1 - \nu_{xy} \nu_{yx}}$, $\bar{A}_{22} = \frac{t_s E_y}{1 - \nu_{xy} \nu_{yx}}$, $\bar{A}_{66} = 2t_s G_{xy}$, lb/in.

AR $= a/b$, plate aspect ratio

a length of plate, in.

a_{mnkl}^{ij} coefficient of characteristic equation

B_{mn} Fourier coefficient of trial function for γ_{xz} , in/in.

b width of plate, in.

C_{mn} Fourier coefficient of trial function for γ_{yz} , in/in.

D_{ij} bending stiffness of plate, $D_{11} = \frac{E_x I_s}{1 - \nu_{xy} \nu_{yx}}$, $D_{12} = \frac{\nu_{yx} E_x I_s}{1 - \nu_{xy} \nu_{yx}}$, $D_{21} = \frac{\nu_{xy} E_y I_s}{1 - \nu_{xy} \nu_{yx}}$,

$D_{22} = \frac{E_y I_s}{1 - \nu_{xy} \nu_{yx}}$, $D_{66} = 2G_{xy}I_s$, in-lb

D_{Qx} D_{Qy} transverse shear stiffness in xz -, yz -planes, lb/in.

E	Young's modulus, lb/in ²
E_x, E_y	Young's modulus, lb/in ²
G_{xy}	shear modulus, lb/in ²
I_s	moment of inertia, per unit width, with respect to plate centroidal axis, $I_s = \frac{1}{12}t_s^3$, in ⁴ /in.
i	index, 1, 2, 3,....
j	index, 1, 2, 3,....
k	index, 1, 2, 3,....
l	index, 1, 2, 3,....
m	index, 1, 2, 3,...., number of buckle half waves in x -direction
N_x^T, N_y^T, N_{xy}^T	thermal forces, lb/in.
n	index, 1, 2, 3,...., number of buckle half waves in y -direction
T	temperature (measured from room temperature), °F
T_c	temperature for constant temperature profile heating, °F
T_m	material temperature
T_o	peak temperature of dome-shaped (or roof-shaped) temperature profile heating, °F
T_s	boundary heat sink temperature, °F
t_s	thickness of plate, in.
u	x -displacement, in.
v	y -displacement, in.
w	out-of-plane displacement, in.
x, y, z	rectangular Cartesian coordinates
$\alpha, \alpha_x, \alpha_y$	coefficient of thermal expansion, in/in-°F
α_{xy}	coefficient of thermal shear distortion, in/in-°F
γ_{xz}, γ_{yz}	transverse shear strain in xz - and yz -planes, in/in.
ξ	numerical factor in buckling equation written for specified panel edge condition
η	$= (T_o)_{cr}/(T_c)_{cr}$, “buckling temperature magnification factor of the first kind” = buckling temperature $(T_o)_{cr}$ of dome temperature loading case (fixed or free support condition) divided by the buckling temperature $(T_c)_{cr}$ of uniform temperature loading case (fixed boundaries)
λ_c	thermal buckling eigenvalue associated with constant temperature profile heating
λ_o	thermal buckling eigenvalue associated with dome-shaped (or roof-shaped) profile heating
ν	Poisson ratio

ξ = $[(T_o)_{cr}]_{T_s \neq 0} / [(T_o)_{cr}]_{T_s = 0}$ “buckling temperature magnification factor of the second kind” = buckling temperature $(T_o)_{cr}$ of dome temperature loading case with any heat sink temperature $T_s \neq 0$ (free support condition) divided by the buckling temperature $(T_o)_{cr}$ of dome temperature loading case with zero heat sink temperature $T_s = 0$ (free support condition)

ρ	density, lb/in ³
σ_T	tensile strength, lb/in ²
σ_x	stress in x -direction, lb/in ²
σ_Y	yield stress, lb/in ²
σ_y	stress in y -direction, lb/in ²
τ	shear stress, lb/in ²
$(\cdot)_{cr}$	critical value at buckling

INTRODUCTION

Hypersonic aircraft are subjected to severe aerodynamic heating during flights. To maintain the structural integrity under high temperature environment, the vehicle structural design concepts of hypersonic flight vehicles are different from those of low Mach number aircraft. Depending on the operating temperature range, vehicle structures may be called “hot” structures or “warm” structures. The “hot” structures fabricated with high temperature alloys can operate at elevated temperatures in the range of 1000 °F to 1500 °F. If fabricated with the carbon/carbon composite material, the operating temperature of the “hot” structures could go as high as 3000 °F. Typical candidate “hot” structural components for hypersonic flight vehicles are hat-stiffened panels fabricated with either monolithic titanium alloys or metal-matrix composite materials; honeycomb sandwich panels fabricated with super-alloy; and carbon/carbon composite elevon (or body flap).

The “warm” structures are fabricated with lightweight materials, such as aluminum, and can operate only up to moderate temperature limit of 350 °F. The space shuttle orbiter is a good example of the “warm” structure. The entire vehicle is protected with the thermal protection system (TPS) to shield the aluminum substructure from overheating beyond the “warm” temperature limit.

Hot structural panels are usually fastened to the cooler substructures that function as heat sinks because of less heating. Thus, even under the uniform surface heat flux, the temperature distribution over the hot structural panels will not be uniform but looks like camel-humped shape (refs. 1–3). This camel-humped shaped temperature distribution is always observed in supported hot structural panels. The buckling behavior of the panel with heat sinks is therefore quite different from the case without heat sinks. Earlier Ko extensively studied thermal buckling problems of hot structural panels under uniform temperature profile heating (without heat sinks effects) (refs. 4–10).

This report studies the thermal buckling behavior of rectangular panels under different types of humped-shaped temperature profile heating to simulate the existence of the supporting boundary heat sink and also studies the effect of the heat sink temperature on the panel buckling temperature. The results are compared to the results of uniform temperature profile heating cases without the heat sink effect.

HUMPED TEMPERATURE PROFILES

Under uniform surface heating, because of the existence of the supporting cooler boundary heat sinks, experimental data have shown that the temperature distribution over a hot structural panel is usually flattened-dome shaped (fig. 1, ref. 1). For performing thermostructural analysis, the actual temperature profile may be idealized with simple mathematical surfaces such as dome-shaped or roof-shaped temperature profiles described in the following sections.

Dome-Shaped Temperature Profile

The dome-shaped temperature profile for a rectangular panel (length a , width b , thickness t_s) is described by the following mathematical function:

$$T(x, y) = T_s + (T_o - T_s) \sin \frac{\pi x}{a} \sin \frac{\pi y}{b} \quad (1)$$

where T_o is the peak temperature at the panel center and T_s is the boundary heat sink temperature (fig. 2). Equation (1) gives a “sine-sine” surface elevated upward by an amount T_s (fig. 2). Keep in mind that the temperatures in this report are the temperature differentials above the room temperature.

Equation (1) is the first-order approximation of the actual temperature profile (fig. 1). For more accurate representation of the actual temperature profile, double Fourier series representation is necessary; however, this representation is not the scope of the present report.

When the boundary temperature T_s goes to zero (fig. 3), equation (1) becomes:

$$T(x, y) = T_o \sin \frac{\pi x}{a} \sin \frac{\pi y}{b} \quad (2)$$

In order to obtain closed-form buckling solutions by means of the minimum potential energy theory, the functional form given by equation (2) is used for dome-shaped temperature loading.

For a special case of uniform temperature profile heating (fig. 4), equation (1) degenerates into:

$$T(x, y) = T_o = T_s = T_c \quad (3)$$

Thermal buckling problems of rectangular sandwich panels under the constant temperature profile heating [eq. (3), fig. 4] was analyzed earlier by Ko (refs. 4–7) using the minimum potential energy theory and finite-element method.

Roof-Shaped Temperature Profile

The actual dome-shaped temperature profile (fig. 1) may also be approximated by a simple temperature distribution surface called roof-shaped temperature profile (peak temperature T_o at the profile central flat zone and boundary heat sink temperature T_s) (figs. 5 and 6). When $T_o = T_s$, the roof-shaped temperature profile also degenerates into uniform temperature profile (fig. 4).

PROBLEMS INVESTIGATED

This report investigated thermal buckling behavior of rectangular panels (length a , width b , thickness t_s) heated under the dome-shaped (figs. 2 and 3) and roof-shaped (figs. 5 and 6) temperature profiles. The main aspects of this research are:

1. To study the effect of the dome-shaped (or roof-shaped) temperature profile on the buckling behavior of the rectangular panels with fixed edges. Then, the study will establish the “buckling temperature magnification factor of the first kind” to scale up the buckling solution of uniform temperature profile heating case to give the buckling solution of the dome-/roof-shaped temperature profile heating case.
2. To study the effect of the heat sink temperatures on the buckling temperatures of rectangular panels with free edges under dome-shaped (or roof-shaped) temperature profile heating. Then, the study will establish the “buckling temperature magnification factor of the second kind” to scale up the buckling solution of dome (or roof) temperature loading case with unheated boundary heat sinks to give the buckling solutions when the boundary heat sinks are heated up.

FINITE-ELEMENT BUCKLING ANALYSIS

This research will use the Structural Performance and Resizing (SPAR) finite-element computer program (ref. 11) to conduct the linear elastic thermal buckling analysis of the rectangular panels.

Panel Geometry

All the rectangular panels analyzed have thickness $t_s = 0.09$ in. with the different dimensions in length a and width b listed in Table 1.

Table 1. Dimensions of rectangular panels; $t_s = 0.09$ in.

a , in.	b , in.	a/b
6	6	1.0
9	6	1.5
12	6	2.0

Figure 7 shows the quarter model generated for the rectangular panel. The quarter model has 625 joint locations (JLOCs) and 576 E43 four-node plate elements.

Material Properties

The rectangular panels are made of high temperature alloy Haynes® 230® (Haynes International, Koyomo, Indiana) with the room temperature properties listed in Table 2.

Table 2. Material properties of Haynes 230 alloy at room temperature.

E	30.6×10^6 lb/in ²
ν	0.31
ρ	0.324 lb/in ³
α	7.0×10^{-6} in/in·°F

Haynes 230 high temperature alloy was used in the fabrication of Hyper-X (X-43) hypersonic research vehicle for Mach 7–10 mission (ref. 3). Appendix A gives the temperature-dependent material properties of Haynes 230 alloy.

Boundary Conditions

The following different panel boundary conditions were considered in the finite-element analysis:

1. 4S fixed — four edges simply supported, with no in-plane displacements [fig. 8(a)].
 - a. $u(x, y) \neq 0, v(x, y) \neq 0$ everywhere except boundaries.
 - b. $u(x, y) = 0, v(x, y) = 0$ everywhere in the panel.
2. 4S free — four edges simply supported and slides freely along the lubricated guides, which can have free in-plane motions [fig. 8(b)].
3. 4C fixed — four edges clamped, with no in-plane displacements [fig. 9(a)].
 - a. $u(x, y) \neq 0, v(x, y) \neq 0$ everywhere except boundaries.
 - b. $u(x, y) = 0, v(x, y) = 0$ everywhere in the panel.
4. 4C free — four edges clamped and slides freely along the lubricated clamping guides, which can have free in-plane motions [fig. 9(b)].

Thermal Loads

The thermal load inputs used for the dome (or roof) temperature loading and constant temperature loading are as follows.

1. Dome-Shaped (or Roof-Shaped) Temperature Profile Heating

For the dome-shaped [eqs. (1) and (2), figs. 2 and 3] and roof-shaped (figs. 5 and 6) temperature load inputs to the SPAR program for the eigenvalue calculations, the unit peak temperature $T_o = 1$ °F was used. The heat sink temperature T_s was allowed to vary over the range $T_s/T_o = 0\text{--}1$ (i.e., $T_s/T_o = 0, 0.1, 0.2, 0.3, 0.4, 0.5, 0.6, 0.7, 0.8, 0.9, 1.0$). Then the eigenvalue (scaling factor) λ_o calculated from SPAR program will give the buckling temperature $(T_o)_{cr}$, namely:

$$(T_o)_{cr} = \lambda_o \times 1 = \lambda_o \quad (4)$$

If the input peak temperature T_o is doubled (i.e., $T_o = 2$ °F), then the calculated eigenvalue will be reduced to half of λ_o given in equation (4) because the product $(T_o \times \lambda_o)$ remains constant.

The reason for using the whole range of $T_s/T_o = 0\sim 1$ is to study the effect of the heat sink temperature T_s on the panel buckling temperature $(T_o)_{cr}$ when the panel edges are free to move. Keep in mind that the panel buckling temperature $(T_o)_{cr}$ will increase with the increasing heat sink temperature T_s because of relaxation of thermal expansion constraint exerted on the panel by the boundary heat sink.

2. Uniform Temperature Profile Heating

As mentioned earlier, the uniform-temperature loading case (fig. 4) is a degenerative case of dome-shaped (or roof-shaped) temperature profile heating. Temperature load of $T_c = 1$ °F is chosen as input to all nodes of the finite-element model so that the eigenvalue λ_c calculated from SPAR program will give the buckling temperature $(T_c)_{cr}$, namely:

$$(T_c)_{cr} = \lambda_c \times 1 = \lambda_c \quad (5)$$

This buckling solution is for the panels with fixed boundary supports. When the panel boundaries can have free in-plane motions (free supports), the constant temperature loading case obviously can never induce thermal buckling (i.e., buckling temperature goes to infinity).

3. Material Property Iterations

In the calculations of buckling temperatures, material property iterations are required to obtain accurate buckling temperatures. Namely, the material properties at certain assumed material temperature T_m must be updated until T_m matches the calculated buckling temperature $(T_c)_{cr}$. Reference 12 discusses in detail this iteration process. Usually it takes only two to three material iterations to yield accurate buckling temperatures.

BUCKLING TEMPERATURE MAGNIFICATION FACTORS

As discussed later in this report, for the fixed supports (4S or 4C) [figs. 8(a) or 9(a)], the buckling temperature $(T_o)_{cr}$ for the dome (or roof) temperature loading case is much higher than the buckling temperature $(T_c)_{cr}$ of the uniform temperature loading case. Therefore, a “buckling temperature magnification factor of the first kind, η ” defined as:

$$\eta = \frac{(T_o)_{cr}}{(T_c)_{cr}} \quad (6)$$

will be used to indicate how many times the buckling temperature $(T_o)_{cr}$ of the dome (or roof) temperature loading case (fixed supports) is magnified from the buckling temperature $(T_c)_{cr}$ of the uniform temperature loading case with fixed supports (fundamental case).

In reality, the hot panel attempts to expand under heating; but its expansion is resisted by the cooler boundary substructures (heat sinks) that expand less. This boundary constraint is the cause of thermal buckling of the panels. Such substructure constraints will gradually relax as the substructures are heated up, resulting in higher panel buckling temperature. In order to discover how the heat sink temperature T_s affects the panel buckling temperature

$(T_o)_{cr}$ for the dome (or roof) temperature loading case with free supports, another ‘‘buckling temperature magnification factor of the second kind, ξ ’ defined as:

$$\xi = \frac{\left[(T_o)_{cr} \right]_{T_s \neq 0}}{\left[(T_o)_{cr} \right]_{T_s = 0}} \quad (7)$$

will be used to indicate how many times the buckling temperature $(T_o)_{cr}$ for the dome (or roof) temperature loading case with free support (4S or 4C) is magnified when the heat sink temperature T_s increases from $T_s = 0$ (no heat sink thermal expansion) to certain nonzero value $T_s \neq 0$ (with heat sink thermal expansion).

MINIMUM POTENTIAL ENERGY BUCKLING ANALYSIS

When the $\{u, v\}$ displacements are zero everywhere in the plate including the boundaries (4S fixed-b and 4C fixed-b cases), the dome-shaped temperature profile heating [eq. (2), fig. 3] will generate identical dome-shaped biaxial stress distributions with no shear stresses. Because of this ideal condition, it is possible to obtain closed-form buckling solutions for this particular case using the minimum potential energy theory.

Energy Equations

Strain energy associated with bending V_1 may be written as (refs. 5 and 6):

$$V_1 = \int_0^a \int_0^b \left\{ \frac{D_{11}}{2} \left[\frac{\partial}{\partial x} \left(\frac{\partial w}{\partial x} - \gamma_{xz} \right) \right]^2 + D_{12} \left[\frac{\partial}{\partial x} \left(\frac{\partial w}{\partial x} - \gamma_{xz} \right) \right] \left[\frac{\partial}{\partial y} \left(\frac{\partial w}{\partial y} - \gamma_{yz} \right) \right] \right. \\ \left. + \frac{D_{22}}{2} \left[\frac{\partial}{\partial y} \left(\frac{\partial w}{\partial y} - \gamma_{yz} \right) \right]^2 + \frac{D_{66}}{2} \left[\frac{\partial}{\partial y} \left(\frac{\partial w}{\partial x} - \gamma_{xz} \right) + \frac{\partial}{\partial x} \left(\frac{\partial w}{\partial y} - \gamma_{yz} \right) \right]^2 + \frac{D_{Qx}}{2} \gamma_{xz}^2 + \frac{D_{Qy}}{2} \gamma_{yz}^2 \right\} dx dy \quad (8)$$

and the strain energy associated with thermal loading V_2 is given by:

$$V_2 = -\frac{1}{2} \int_0^a \int_0^b \left[N_x^T \left(\frac{\partial w}{\partial x} \right)^2 + 2N_{xy}^T \left(\frac{\partial w}{\partial x} \right) \left(\frac{\partial w}{\partial y} \right) + N_y^T \left(\frac{\partial w}{\partial y} \right)^2 \right] dx dy \quad (9)$$

The dome-shaped temperature loading functions may be expressed as follows (refs. 5 and 6):

$$N_x^T(x, y) = (\bar{A}_{11}\alpha_x + \bar{A}_{12}\alpha_y)T_o \sin \frac{\pi x}{a} \sin \frac{\pi y}{b} \quad (10)$$

$$N_y^T(x, y) = (\bar{A}_{21}\alpha_x + \bar{A}_{22}\alpha_y)T_o \sin \frac{\pi x}{a} \sin \frac{\pi y}{b} \quad (11)$$

$$N_{xy}^T(x, y) = 0 \quad (12)$$

The preceding thermal loading functions (10)–(12) hold only for the 4S fixed-b and 4C fixed-b cases [i.e., $u(x, y) = 0$, $v(x, y) = 0$ everywhere].

For other fixed panel cases under dome temperature heating, the in-plane displacements of panel interior points are nonzero [i.e., $u(x, y) \neq 0$, $v(x, y) \neq 0$], and the thermal loads $\{N_x^T, N_y^T, N_{xy}^T\}$ are complicated functions of $\{x, y\}$; and thus it will be too cumbersome to apply the minimum potential energy method. Therefore, SPAR was used to obtain quick buckling solutions.

Deformation Functions

The deformation functions for the 4S fixed-b case and 4C fixed-b case may be expressed in the following forms (refs. 5 and 6).

Case 1. Four edges simply supported (4S fixed-b case)

$$w(x, y) = \sum_{m=1}^{\infty} \sum_{n=1}^{\infty} A_{mn} \sin \frac{m\pi x}{a} \sin \frac{n\pi y}{b} \quad (13)$$

$$\gamma_{xz}(x, y) = \sum_{m=1}^{\infty} \sum_{n=1}^{\infty} B_{mn} \cos \frac{m\pi x}{a} \sin \frac{n\pi y}{b} \quad (14)$$

$$\gamma_{yz}(x, y) = \sum_{m=1}^{\infty} \sum_{n=1}^{\infty} C_{mn} \sin \frac{m\pi x}{a} \cos \frac{n\pi y}{b} \quad (15)$$

Case 2. Four edges clamped (4C fixed-b case)

$$w(x, y) = \sin \frac{\pi x}{a} \sin \frac{\pi y}{b} \sum_{m=1}^{\infty} \sum_{n=1}^{\infty} A_{mn} \sin \frac{m\pi x}{a} \sin \frac{n\pi y}{b} \quad (16)$$

$$\begin{aligned} \gamma_{xz}(x, y) = & \cos \frac{\pi x}{a} \sin \frac{\pi y}{b} \sum_{m=1}^{\infty} \sum_{n=1}^{\infty} B_{mn} \sin \frac{m\pi x}{a} \sin \frac{n\pi y}{b} \\ & + \sin \frac{\pi x}{a} \sin \frac{\pi y}{b} \sum_{m=1}^{\infty} \sum_{n=1}^{\infty} mB_{mn} \cos \frac{m\pi x}{a} \sin \frac{n\pi y}{b} \end{aligned} \quad (17)$$

$$\begin{aligned} \gamma_{yz}(x, y) = & \sin \frac{\pi x}{a} \cos \frac{\pi y}{b} \sum_{m=1}^{\infty} \sum_{n=1}^{\infty} C_{mn} \sin \frac{m\pi x}{a} \sin \frac{n\pi y}{b} \\ & + \sin \frac{\pi x}{a} \sin \frac{\pi y}{b} \sum_{m=1}^{\infty} \sum_{n=1}^{\infty} nC_{mn} \sin \frac{m\pi x}{a} \cos \frac{n\pi y}{b} \end{aligned} \quad (18)$$

Buckling Equations

Application of the minimum potential energy theory yields the following homogeneous simultaneous characteristic equations (refs. 5 and 6) for each set of integral values $\{m, n\}$ (or mode shape) written for orthotropic rectangular panels under dome-shaped temperature profile heating [eq. (2)]:

$$\sum_k \sum_l \left[\frac{M_{mnkl}}{T_o} + P_{mnkl} \right] A_{kl} = 0 \quad (19)$$

where the stiffness/geometry parameter M_{mnkl} is given by:

$$M_{mnkl} = \frac{1}{\zeta} \left[a_{mnkl}^{11} + \frac{a_{mnkl}^{12}(a_{mnkl}^{23}a_{mnkl}^{31} - a_{mnkl}^{21}a_{mnkl}^{33}) + a_{mnkl}^{13}(a_{mnkl}^{21}a_{mnkl}^{32} - a_{mnkl}^{22}a_{mnkl}^{31})}{a_{mnkl}^{22}a_{mnkl}^{33} - a_{mnkl}^{23}a_{mnkl}^{32}} \right] \quad (20)$$

and where a_{mnkl}^{ij} are the coefficients of characteristic equations.

Appendix B gives functional expressions of a_{mnkl}^{ij} , which is taken from Appendix C of reference 6 (or Appendix A of ref. 7) with the loading terms containing $\{k_x, k_y\}$ removed.

For the simply-supported edges (4S fixed-b case), the value of ζ in equation (20) is $\zeta = 32$; and the thermal forcing term P_{mnkl} in equation (19) has the following form (special integrals given in Appendix C were used in the calculations).

$$P_{mnkl} = - \left[(\bar{A}_{11}\alpha_x + \bar{A}_{12}\alpha_y) \frac{(m^2 + k^2) - 1}{a^2} + (\bar{A}_{21}\alpha_x + \bar{A}_{22}\alpha_y) \frac{(n^2 + l^2) - 1}{b^2} \right] \times \left\{ \frac{mnkl}{[(m+k)^2 - 1][(m-k)^2 - 1][(n+l)^2 - 1][(n-l)^2 - 1]} \right\} \quad (21)$$

$$m \pm k = \text{even}, n \pm l = \text{even}$$

For the clamped edges (4C fixed-b case), the value of ζ in equation (20) is $\zeta = 24$, and P_{mnkl} in equation (19) takes on the following form (special integrals given in Appendix C were used in the calculations).

$$P_{mnkl} = \frac{mnkl}{a^2} (A_{11}a_x + A_{12}a_y) \left\{ \frac{3(m^2 + k^2) + 1}{[(m+k)^2 - 1][(m-k)^2 - 1]} - \frac{3[(m^2 + k^2) - 5]}{[(m+k)^2 - 9][(m-k)^2 - 9]} \right\} + \frac{mnkl}{b^2} (A_{21}a_x + A_{22}a_y) \left\{ \frac{3(n^2 + l^2) + 1}{[(n+l)^2 - 1][(n-l)^2 - 1]} - \frac{3[(n^2 + l^2) - 5]}{[(n+l)^2 - 9][(n-l)^2 - 9]} \right\} \times \left\{ \frac{-1}{[(m+k)^2 - 1][(m-k)^2 - 1]} + \frac{1}{[(m+k)^2 - 9][(m-k)^2 - 9]} \right\}$$

$$m \pm k = \text{even}, n \pm l = \text{even}$$

For the unknown deflection coefficients A_{kl} in equation (19) to have nontrivial solution, the determinant of the coefficients of unknown A_{kl} of simultaneous equations written out from equation (19) must be set to zero for eigenvalue extractions. The largest eigenvalue ($1/T_o$) will then give the lowest critical buckling temperature (T_o)_{cr}.

Appendix D shows the determinants of the coefficients of simultaneous equation (called buckling equations) written out from equation (19) up to order 12 for the cases $m \pm n = \text{even}$ (symmetrical buckling) and $m \pm n = \text{odd}$ (antisymmetrical buckling) for the 4S and 4C cases. The symmetrical buckling case ($m \pm n = \text{even}$) gives the lowest buckling temperature (T_o)_{cr} associated with the lowest buckling mode.

Buckling Temperatures for Isotropic Cases

The purpose of the present buckling analysis is to study the effect of dome-shaped temperature profile heating on the buckling of the rectangular panels and not the effect of material anisotropy. Therefore, only the isotropic panels are considered.

1. Simply-Supported Edges

For the simply-supported case (4S fixed-b case) ignoring the transverse shear effect, M_{mnkl} [eq. (20)] and P_{mnkl} [eq. (21)] take on the following forms:

$$M_{mnkl} = \frac{Et_s^3 \pi^4}{384(1-\nu^2)} \left(\frac{m^2}{a^2} + \frac{n^2}{b^2} \right) \quad (23)$$

$$P_{mnkl} = -\frac{Et_s \alpha}{1-\nu} \left[\frac{(m^2 + k^2) - 1}{a^2} + \frac{(n^2 + l^2) - 1}{b^2} \right] \quad (24)$$

$$\times \left\{ \frac{mnkl}{[(m+k)^2 - 1][(m-k)^2 - 1][(n+l)^2 - 1][(n-l)^2 - 1]} \right\}$$

$$m \pm k = \text{even}, n \pm l = \text{even}$$

The first-order solution ($m = n = k = l = 1$) of the buckling temperature (T_o)_{cr} for the dome-shaped heating may be calculated through combining equations (19), (23), and (24) by setting $m = n = k = l = 1$.

$$(T_o)_{cr} = \frac{3\pi^4 t_s^2}{128\alpha(1+\nu)} \left(\frac{1}{a^2} + \frac{1}{b^2} \right) \quad (25)$$

For the constant temperature heating case, the first-order ($m = 1, n = 1$) buckling temperature (T_c)_{cr} for the isotropic panel can be calculated from equations (28)–(30) of reference 7. With the transverse shear effect neglected, the first-order buckling temperature (T_c)_{cr} for this case has the following form:

$$(T_c)_{cr} = \frac{\pi^2 t_s^2}{12\alpha(1+\nu)} \left(\frac{1}{a^2} + \frac{1}{b^2} \right) \quad (26)$$

Dividing equation (25) by equation (26) yields the buckling temperature magnification factor of the first kind η for the simply-supported first-order case ($m = n = k = l = 1$) in a neat form:

$$\eta = \frac{(T_o)_{cr}}{(T_c)_{cr}} = \frac{9\pi^2}{32} = 2.7758 \quad (27)$$

that is independent of panel aspect ratio.

For the 4S case, the values of η based on the second and third-order buckling solutions (which depend on the aspect ratio a/b) were also obtained. The RESULTS section presents these values.

2. Clamped Edges

For the clamped case (4C fixed-b case), the first-order solution ($m = n = k = l = 1$) for the “dome-shaped” temperature case is:

$$M_{1111} = \frac{\pi^4 E t_s^3}{24(1-\nu^2)} \left(\frac{1}{a^4} + \frac{2}{3} \frac{1}{a^2 b^2} + \frac{1}{b^4} \right) \quad (28)$$

$$P_{1111} = -\frac{512}{675(1-\nu)} \frac{E \alpha t_s}{a} \left(\frac{1}{a^2} + \frac{1}{b^2} \right) \quad (29)$$

The first-order solution ($m = n = k = l = 1$) of the buckling temperature $(T_o)_{cr}$ for the clamped panel under the dome-shaped heating may be calculated by combining equations (19), (28), and (29) to yield:

$$(T_o)_{cr} = \frac{75\pi^4 t_s^2}{64^2 \alpha(1+\nu)} \frac{\left(\frac{3}{a^4} + \frac{2}{a^2 b^2} + \frac{3}{b^4} \right)}{\left(\frac{1}{a^2} + \frac{1}{b^2} \right)} \quad (30)$$

The first-order solution ($m = n = k = l = 1$) for the constant temperature case calculated from equations (28)–(30) of reference 7 gives:

$$(T_c)_{cr} = \frac{\pi^2 t_s^2}{9\alpha(1+\nu)} \frac{\left(\frac{3}{a^4} + \frac{2}{a^2 b^2} + \frac{3}{b^4} \right)}{\left(\frac{1}{a^2} + \frac{1}{b^2} \right)} \quad (31)$$

The ratio of equations (30) and (31) gives the buckling temperature magnification factor of the first kind η for the 4C case first-order solution ($m = n = k = l = 1$) in a neat closed form as:

$$\eta = \frac{(T_o)_{cr}}{(T_c)_{cr}} = \frac{3 \times 15^2 \pi^2}{64^2} = 1.6265 \quad (32)$$

which, similar to the 4S case [eq. (27)], is also independent of panel aspect ratio. As discussed in a following section, for the 4C case, the first-order buckling solution gives a quite accurate value of η . Therefore, higher order values of η were not calculated.

RESULTS

The following sections present the results of the thermal buckling analyses of the rectangular plates under different heating profiles.

Buckling Temperature Magnification Factors

Figures 10 and 11 show the buckled shapes of the isotropic square panel ($a/b = 1$) under different temperature profile loading and under different boundary conditions. Notice that the panel buckling shapes are insensitive to the temperature loading functions for each set of edge conditions.

Table 3 lists the buckling temperature magnification factor of the first kind $\eta = (T_o)_{cr}/(T_c)_{cr}$ calculated from SPAR program for the isotropic rectangular panels with different aspect ratios under dome-shaped temperature profile heating with zero heat sink temperature [$T_s = 0$, eq. (2)].

Table 3. Buckling temperature magnification factor η for rectangular plates under dome-shaped temperature profile heating; $T_s = 0$; fixed boundaries.

BC \ a/b	η		
	1	1.5	2
4S	1.9721 (2.0034)	1.9603	1.9453
4C	1.8035 (1.8299)	1.7848	1.7320

() Sandwich panel (ref. 7).

Notice that η is insensitive to the change of panel aspect ratio a/b and that the 4S cases have slightly higher values of η than the 4C cases.

In Table 3, the η values for the square sandwich panel ($a/b = 1$) are also shown in the parentheses. Those values were calculated from the previous SPAR program developed for the buckling of sandwich panel (ref. 7). Notice the proximity of the η values for solid and sandwich panels.

Table 4 compares the values of η calculated from the minimum potential energy theory and from the SPAR program for the special case of square panel ($a/b = 1$) under the dome-shaped temperature profile heating [$T_s = 0$, eq. (2), fig. 3], and with constraint $u = v = 0$ everywhere.

Table 4. Buckling temperature magnification factor η for square plate ($a/b = 1$) under dome-shaped temperature profile heating; $T_s = 0$; $u = v = 0$ everywhere.

BC Method	η		
	Ko theory	SPAR	Percent difference
4S	2.4503***	2.5185	2.71
	(2.6394)**	4.80
	(2.7758)*	10.22
4C	1.6265*	1.5993	1.70

* First-order solution.

** Second-order solution.

*** Third-order solution.

For the 4S case, the η values were hand calculated up to the third-order buckling solutions. The third-order solution compares quite well with the SPAR solution with only 2.71 percent difference. Thus, higher order solutions were not pursued.

For the 4C case, the first-order solution is extremely good with only 1.70 percent difference compared with the SPAR solution. Therefore, higher order solutions for η were not calculated.

Table 5 lists the buckling temperatures $(T_o)_{cr}$ and the values of buckling temperature magnification factors $\{\eta, \xi\}$ calculated for the simply-supported (4S fixed/free) square panel ($a/b = 1$) under shifted dome-shaped temperature loading [eq. (1), fig. 2] under different heat sink temperatures T_s .

Table 5. Buckling temperatures of square plate ($a/b = 1$) under dome-shaped temperature profile heating; 4S fixed and free cases.

T_s/T_o	4S Fixed		4S Free	
	$(T_o)_{cr}$, °F	η	$(T_o)_{cr}$, °F	ξ
0.0	80	2.00	515	1.00
0.1	73	1.83	568	1.10
0.2	67	1.68	635	1.23
0.3	62	1.55	718	1.39
0.4	57	1.43	821	1.59
0.5	54	1.35	960	1.86
0.6	50	1.25	1,175	2.28
0.7	47	1.18	1,500	2.91
0.8	45	1.13	2,070	4.02
0.9	42	1.05	(4,213)	8.18
1.0*	40	1.00	∞	∞

* Uniform temperature loading.

() Exceeded melting range 2,375 °F~2,500 °F of Haynes 230 alloy.

Note that for the 4S fixed edges, the value of η decreases with the increasing heat sink temperature T_s . For the 4S free edge case, ξ increases with the increasing heat sink temperature T_s . When $T_s/T_o = 1$, the case degenerated into the uniform temperature loading case for which the buckling temperature goes to infinity for the 4S free edge case (i.e., thermal buckling does not occur).

It must be mentioned that for the actual hot sandwich panel (ref. 1) $T_s/T_o = 0.45$ and for the HYPER-X wing panel (ref. 3) $T_s/T_o = 0.54$.

Table 6 lists the buckling temperatures $(T_o)_{cr}$ and the values of buckling temperature magnification factors $\{\eta, \xi\}$ calculated for the clamped (4C fixed/free) square panel ($a/b = 1$) under shifted dome-shaped temperature loading [eq. (1), fig. 2] and under different heat sink temperatures T_s .

Table 6. Buckling temperatures of square plate ($a/b = 1$) under dome-shaped temperature profile heating; 4C fixed and free cases.

T_s/T_o	4C Fixed		4C Free	
	$(T_o)_{cr}$, °F	η	$(T_o)_{cr}$, °F	ξ
0.0	194	1.81	810	1.00
0.1	180	1.68	886	1.09
0.2	167	1.56	982	1.20
0.3	156	1.46	1,110	1.34
0.4	147	1.37	1,272	1.57
0.5	138	1.29	1,480	1.83
0.6	130	1.21	1,770	2.19
0.7	124	1.16	2,302	2.84
0.8	118	1.10	(3,581)	4.42
0.9	112	1.05	(6,907)	8.53
1.0*	107	1.00	∞	∞

* Uniform temperature profile heating.

() Exceeded melting range 2,375 °F~2,500 °F of Haynes 230 alloy.

Note that for the 4C fixed case, similar to the 4S fixed case, value of η decreases with the increasing heat sink temperature T_o . For the 4C free case, the values of ξ are very close to the corresponding ξ value of 4S free case (Table 5). Again, when T_s reaches T_o (i.e., $T_s/T_o = 1$), the case degenerated into the uniform temperature loading case for which the buckling temperature goes to infinity for the 4C free case (i.e., no thermal buckling).

Table 7 lists the buckling temperatures $(T_o)_{cr}$ and the values of buckling temperature magnification factors $\{\eta, \xi\}$ calculated for the simply-supported (4S fixed/free) square panel ($a/b = 1$) under shifted roof-shaped temperature loading (fig. 5) under different heat sink temperatures T_s .

Table 7. Buckling temperatures of square plate ($a/b = 1$) under roof-shaped temperature profile heating; 4S fixed and free cases.

T_s/T_o	4S Fixed		4S Free	
	$(T_o)_{cr}$, °F	η	$(T_o)_{cr}$, °F	ξ
0.0	51	1.28	622	1.00
0.1	50	1.25	690	1.11
0.2	48	1.20	767	1.23
0.3	47	1.18	860	1.38
0.4	46	1.15	985	1.58
0.5	45	1.13	1,160	1.86
0.6	44	1.10	1,410	2.27
0.7	43	1.08	1,764	2.84
0.8	42	1.05	(2,587)	4.16
0.9	41	1.03	(5,174)	8.32
1.0*	40	1.00	∞	∞

* Uniform temperature profile heating.

() Exceeded melting range 2,375 °F~2,500 °F of Haynes 230 alloy.

Table 8 lists the buckling temperatures $(T_o)_{cr}$ and the values of buckling temperature magnification factors $\{\eta, \xi\}$ calculated for the clamped (4C fixed/free) square panel ($a/b = 1$) under shifted roof-shaped temperature loading (fig. 5) under different heat sink temperatures T_s .

Table 8. Buckling temperatures of square plate ($a/b = 1$) under roof-shaped temperature profile heating; 4C fixed and free cases.

T_s/T_o	4C Fixed		4C Free	
	$(T_o)_{cr}$, °F	η	$(T_o)_{cr}$, °F	ξ
0.0	132	1.23	1,125	1.00
0.1	129	1.21	1,235	1.10
0.2	126	1.18	1,370	1.22
0.3	123	1.15	1,520	1.35
0.4	121	1.13	1,720	1.53
0.5	118	1.10	1,980	1.76
0.6	116	1.08	(2,501)	2.22
0.7	113	1.06	(3,335)	2.96
0.8	111	1.04	(5,002)	4.45
0.9	109	1.02	(10,004)	8.89
1.0*	107	1.00	∞	∞

* Uniform temperature loading.

() Exceeded melting range 2,375 °F~2,500 °F of Haynes 230 alloy.

Figures 12 and 13, respectively, show the buckling temperatures $(T_o)_{cr}$ (data from tables 5–8) plotted as functions of normalized heat sink temperature T_s/T_o for the fixed and free edge cases to illustrate entirely different buckling behavior of the fixed and free edge cases. Note from figure 12 that for the fixed edges, the buckling temperatures of the roof-shaped temperature profile case are much lower than the dome-shaped temperature profile case for each panel support condition. However, for the free edges (fig. 13), the reverse is true.

Figure 14 shows the buckling temperature magnification factors $\{\eta, \xi\}$ (data from tables 5–8) plotted as functions of normalized heat sink temperature T_s/T_o for easy visualization of the shapes of $\{\eta, \xi\}$ curves. Note that η values for the roof case are much lower than the dome case for the same support condition. For the free edge cases, the ξ curves for different loading and edge support conditions stay very close.

In-Plane Deformations

When the panel is constrained only at the four boundaries, the panel interior points can have in-plane free motions if the temperature loading is nonuniform. Figure 15 shows the in-plane deformed shapes of the square panel under dome-shaped [fig. 15(a)] and roof-shaped [fig. 15(b)] temperature loading cases. As expected, the panel center regions expand more than the panel boundary regions as the result of heating temperature profiles. Figures 16 and 17, respectively, show the distributions of in-plane displacements $u(x,y)$ and $v(x,y)$ for the dome-shaped temperature loading. Note that $\{u, v\}$ reach a maximum at points between the panel center and the boundaries. For the roof-shaped temperature profile case (figs. 18 and 19), the maximum points of $\{u, v\}$ migrated toward the panel center.

Thermal Stresses

Figures 20 and 21, respectively, show the compressive thermal stresses $\{\sigma_x, \sigma_y\}$ induced in a fixed square panel ($a/b = 1$) under the unit dome-shaped temperature profile heating [$T_o = 1$ °F, $T_s = 0$; eq. (2), fig. 3]. Even though the loading temperature profile is dome shaped, the distributions of thermal stresses $\{\sigma_x, \sigma_y\}$ are airplane-hanger shaped because $u(x,y) \neq 0$ and $v(x,y) \neq 0$ within the fixed boundaries. Figure 22 shows the distribution of shear stress τ_{xy} which is wavy shaped. The peak magnitudes of the shear stress occur at the boundaries and near the panel corners.

For the roof-shaped temperature profile heating ($T_o = 1$ °F, $T_s = 0$) (fig. 6), the distributions of $\{\sigma_x, \sigma_y\}$ are roughly trapezoidal hanger-shaped (figs. 23 and 24). The shear stress distribution (fig. 25) exhibits zero shear stress near the panel center region and a maximum shear near each panel corner.

If the in-plane displacements $\{u, v\}$ are constrained everywhere in the panel including the edges [i.e., $u(x,y) = v(x,y) = 0$], the resulting distributions of the biaxial stresses $\{\sigma_x, \sigma_y\}$ will be dome-shaped just like the input dome temperature distribution (figs. 26 and 27), and the in-plane shear stress τ_{xy} diminishes ($\tau_{xy} = 0$). For the case of roof-shaped temperature profile (figs. 28 and 29), the distributions of the biaxial stresses $\{\sigma_x, \sigma_y\}$ reflect the input temperature profile.

Table 9 lists the fundamental thermal stresses induced in the fixed square panel ($a/b = 1$) by the dome-shaped (or roof-shaped) temperature loading ($T_o = 1$ °F) with zero heat sink temperature ($T_s = 0$).

Table 9. Peak thermal stresses $\{\sigma_x, \sigma_y, \tau_{xy}\}$ induced in square plate ($a/b = 1$) under dome-shaped and roof-shaped temperature loads; $T_o = 1$ °F; $T_s = 0$; fixed boundaries.

Constraints of $\{u, v\}$	Heating	σ_x , lb/in ²	σ_y , lb/in ²	τ_{xy} , lb/in ²
$u = 0, v = 0$, edges only	Dome	-189.26	-189.26	31.27
	Roof	-256.38	-256.38	48.66
$u = 0, v = 0$, everywhere	Dome	-301.05	-301.05	0.00
	Roof	-306.77	-306.77	0.00

Note that by setting $u(x,y) = v(x,y) = 0$ everywhere in the panel including the boundaries, the peak magnitudes of the biaxial stresses $\{\sigma_x, \sigma_y\}$ were raised respectively by 59 percent and 20 percent for the dome- and roof-shaped temperature profile cases.

CONCLUDING REMARKS

Thermal buckling characteristics of rectangular panels subjected to dome-shaped and roof-shaped temperature profile heating were investigated using the finite-element method and the minimum potential energy method. The key results include:

1. “Buckling temperature magnification factor of the first kind, η ” was established to scale up the buckling solution of uniform temperature loading case to give the buckling solution of the dome-shaped (or roof-shaped) temperature loading cases. Also, “buckling temperature magnification factor of the second kind, ξ ” was established to scale up the buckling solution of dome temperature loading case with unheated boundary heat sinks to give the buckling solutions when the boundary heat sinks are heated up.
2. For the fixed boundary cases when the panel interior in-plane motions are not constrained ($u \neq 0, v \neq 0$ except boundaries), the panel buckling temperatures under dome-shaped temperature loading are practically twice the buckling temperatures of the uniform temperature loading cases.
3. For simply-supported case (4S fixed, $u = v = 0$ everywhere) under the dome-shaped temperature profile heating, the third-order solution of the “buckling temperature magnification factor of the first kind, η ” calculated from the minimum potential energy theory, agrees fairly well with the η value calculated from the finite-element method. The solution difference is only 2.71 percent.
4. For the clamped case (4C fixed, $u = v = 0$ everywhere) under dome-shaped temperature profile heating, the first-order solution of minimum potential energy gives quite accurate value of η with only 1.70 percent difference from the finite-element solution.
5. For the fixed boundary case when the panel interior points can have free in-plane motions ($u \neq 0, v \neq 0$ except boundaries), the distribution profiles of the compressive stresses $\{\sigma_x, \sigma_y\}$ under the dome-shaped (or roof-shaped) temperature loading have airplane-hanger-like shapes.
6. For the fixed boundary case when the panel in-plane motions are constrained everywhere ($u = v = 0$ everywhere), the distribution profiles of the compressive stresses $\{\sigma_x, \sigma_y\}$ take on the dome shape (or roof shape) similar to the input dome-shaped (or roof-shaped) temperature profile.
7. The “buckling temperature magnification factor of the first kind, η ” associated with the dome-shaped temperature profile heating is much greater than that for the roof-shaped temperature profile heating case for both 4S and 4C fixed edge conditions.

8. The “buckling temperature magnification factor of the second kind, ξ ” associated with the dome-shaped and roof-shaped temperature profile heating are very close for 4S and 4C free edge conditions.

*Dryden Flight Research Center
National Aeronautics and Space Administration
Edwards, California, April 3, 2002*

APPENDIX A
TEMPERATURE-DEPENDENT MATERIAL PROPERTIES OF
HAYNES 230 ALLOY

Temperature-dependent material properties of Haynes 230; $\rho = 0.324 \text{ lb/in}^3$.

$T, {}^\circ\text{F}$	$E \times 10^6, \text{lb/in}^2$	$\sigma_T \times 10^3, \text{lb/in}^2$	$\sigma_Y \times 10^3, \text{lb/in}^2$	$\alpha \times 10^{-6}, \text{in/in-}{}^\circ\text{F}$	ν^*
70	30.6	125.4	57.4	7.0	0.310
200	30.1	(122.2)	(55.0)	7.1	0.311
400	29.3	(117.3)	(51.3)	7.2	0.315
600	28.3	(112.3)	(47.7)	7.4	0.318
800	27.3	(107.4)	(44.0)	7.6	0.321
1000	26.4	102.5	40.3	7.9	0.324
1200	25.3	97.7	39.5	8.1	0.330
1400	24.1	87.7	42.5	8.3	0.332
1600	23.1	63.1	37.3	8.6	0.334
1800	21.9	35.2	21.1	8.9	0.340
2000	20.7*	19.5	10.8	9.2*	0.343

* Estimated.

() Interpolated.

APPENDIX B

COEFFICIENTS OF CHARACTERISTIC EQUATIONS

The characteristic coefficients a_{mnkl}^{ij} appearing in equation (20) are defined in the following for different indicial and edge conditions (refs. 6, 7).

Case 1: 4S condition

1. $m = k, n = l$

$$\begin{aligned}
 a_{mnmn}^{11} &= D_{11} \left(\frac{m\pi}{a} \right)^4 + 2(D_{12} + 2D_{66}) \left(\frac{m\pi}{a} \right)^2 \left(\frac{n\pi}{b} \right)^2 + D_{22} \left(\frac{n\pi}{b} \right)^4 \\
 a_{mnmn}^{12} = a_{mnmn}^{21} &= - \left[D_{11} \left(\frac{m\pi}{a} \right)^3 + (D_{12} + 2D_{66}) \left(\frac{m\pi}{a} \right) \left(\frac{n\pi}{b} \right)^2 \right] \\
 a_{mnmn}^{13} = a_{mnmn}^{31} &= - \left[D_{22} \left(\frac{n\pi}{b} \right)^3 + (D_{12} + 2D_{66}) \left(\frac{m\pi}{a} \right)^2 \left(\frac{n\pi}{b} \right) \right] \\
 a_{mnmn}^{22} &= D_{11} \left(\frac{m\pi}{a} \right)^2 + D_{66} \left(\frac{n\pi}{b} \right)^2 + D_{Qx} \\
 a_{mnmn}^{23} = a_{mnmn}^{32} &= (D_{12} + D_{66}) \left(\frac{m\pi}{a} \right) \left(\frac{n\pi}{b} \right) \\
 a_{mnmn}^{33} &= D_{22} \left(\frac{n\pi}{b} \right)^2 + D_{66} \left(\frac{m\pi}{a} \right)^2 + D_{Qy}
 \end{aligned} \tag{B-1}$$

2. $m \neq k, n \neq l$

$$a_{mnkl}^{ij} = 0 \tag{B-2}$$

Case 2: 4C condition

1. $m = n = k = l = 1$

$$\begin{aligned}
 a_{1111}^{11} &= 12D_{11} \left(\frac{\pi}{a} \right)^4 + 8(D_{12} + 2D_{66}) \left(\frac{\pi}{a} \right)^2 \left(\frac{\pi}{b} \right)^2 + 12D_{22} \left(\frac{\pi}{b} \right)^4 \\
 a_{1111}^{12} = a_{1111}^{21} &= - \left[12D_{11} \left(\frac{\pi}{a} \right)^3 + 4(D_{12} + 2D_{66}) \left(\frac{\pi}{a} \right) \left(\frac{\pi}{b} \right)^2 \right] \\
 a_{1111}^{13} = a_{1111}^{31} &= - \left[12D_{22} \left(\frac{\pi}{b} \right)^3 + 4(D_{12} + 2D_{66}) \left(\frac{\pi}{a} \right)^2 \left(\frac{\pi}{b} \right) \right] \\
 a_{1111}^{22} &= 12D_{11} \left(\frac{\pi}{a} \right)^2 + 4D_{66} \left(\frac{\pi}{b} \right)^2 + 3D_{Qx} \\
 a_{1111}^{23} = a_{1111}^{32} &= 4(D_{12} + D_{66}) \left(\frac{\pi}{a} \right) \left(\frac{\pi}{b} \right)
 \end{aligned} \tag{B-3}$$

$$a_{1111}^{33} = 12D_{22}\left(\frac{\pi}{b}\right)^2 + 4D_{66}\left(\frac{\pi}{a}\right)^2 + 3D_{Qy}$$

2. $m = k = 1, n = l \neq 1$

$$a_{1n1n}^{11} = 8D_{11}\left(\frac{\pi}{a}\right)^4 + 4(D_{12} + 2D_{66})\left(\frac{\pi}{a}\right)\left(\frac{\pi}{b}\right)^2(1+n^2) + \frac{3}{2}D_{22}\left(\frac{\pi}{b}\right)^4\left[(1+n^2)^2 + 4n^2\right]$$

$$a_{1n1n}^{12} = a_{1n1n}^{21} = -\left[8D_{11}\left(\frac{\pi}{a}\right)^3 + 2(D_{12} + 2D_{66})\left(\frac{\pi}{a}\right)\left(\frac{\pi}{b}\right)^2(1+n^2)\right]$$

$$a_{1n1n}^{13} = a_{1n1n}^{31} = -\left\{\frac{3}{2}D_{22}\left(\frac{\pi}{b}\right)^3\left[(1+n^2)^2 + 4n^2\right] + 2(D_{12} + 2D_{66})\left(\frac{\pi}{a}\right)^2\left(\frac{\pi}{b}\right)(1+n^2)\right\} \quad (\text{B-4})$$

$$a_{1n1n}^{22} = 8D_{11}\left(\frac{\pi}{a}\right)^2 + 2D_{66}\left(\frac{\pi}{b}\right)^2(1+n^2) + 2D_{Qx}$$

$$a_{1n1n}^{23} = a_{1n1n}^{32} = 2(D_{12} + D_{66})\left(\frac{\pi}{a}\right)\left(\frac{\pi}{b}\right)(1+n^2)$$

$$a_{1n1n}^{33} = \frac{3}{2}D_{22}\left(\frac{\pi}{b}\right)^2\left[(1+n^2)^2 + 4n^2\right] + 2D_{66}\left(\frac{\pi}{a}\right)^2(1+n^2) + \frac{3}{2}D_{Qy}(1+n^2)$$

3. $m = k \neq 1, n = l = 1$

$$a_{m1m1}^{11} = \frac{3}{2}D_{11}\left(\frac{\pi}{a}\right)^4\left[(1+m^2)^2 + 4m^2\right] + 4(D_{12} + 2D_{66})\left(\frac{\pi}{a}\right)^2\left(\frac{\pi}{b}\right)^2(1+m^2) + 8D_{22}\left(\frac{\pi}{b}\right)^4$$

$$a_{m1m1}^{12} = a_{m1m1}^{21} = -\left\{\frac{3}{2}D_{11}\left(\frac{\pi}{a}\right)^3\left[(1+m^2)^2 + 4m^2\right] + 2(D_{12} + 2D_{66})\left(\frac{\pi}{a}\right)\left(\frac{\pi}{b}\right)^2(1+m^2)\right\}$$

$$a_{m1m1}^{13} = a_{m1m1}^{31} = -\left[8D_{22}\left(\frac{\pi}{b}\right)^3 + 2(D_{12} + 2D_{66})\left(\frac{\pi}{a}\right)^2\left(\frac{\pi}{b}\right)(1+m^2)\right] \quad (\text{B-5})$$

$$a_{m1m1}^{22} = \frac{3}{2}D_{11}\left(\frac{\pi}{a}\right)^2\left[(1+m^2)^2 + 4m^2\right] + 2D_{66}\left(\frac{\pi}{b}\right)^2(1+m^2) + \frac{3}{2}D_{Qx}(1+m^2)$$

$$a_{m1m1}^{23} = a_{m1m1}^{32} = 2(D_{12} + D_{66})\left(\frac{\pi}{a}\right)\left(\frac{\pi}{b}\right)(1+m^2)$$

$$a_{m1m1}^{33} = 8D_{22}\left(\frac{\pi}{b}\right)^2 + 2D_{66}\left(\frac{\pi}{a}\right)^2(1+m^2) + 2D_{Qy}$$

4. $m = k \neq 1, n = l \neq 1$

$$a_{mnmn}^{11} = D_{11}\left(\frac{\pi}{a}\right)^4\left[(1+m^2)^2 + 4m^2\right] + 2(D_{12} + 2D_{66})\left(\frac{\pi}{a}\right)^2\left(\frac{\pi}{b}\right)^2(1+m^2)(1+n^2) + D_{22}\left(\frac{\pi}{b}\right)^4\left[(1+n^2)^2 + 4n^2\right]$$

$$\begin{aligned}
a_{mnmn}^{12} &= a_{mnmn}^{21} = - \left\{ D_{11} \left(\frac{\pi}{a} \right)^3 \left[(1+m^2)^2 + 4m^2 \right] + (D_{12} + 2D_{66}) \left(\frac{\pi}{a} \right) \left(\frac{\pi}{b} \right)^2 (1+m^2)(1+n^2) \right\} \\
a_{mnmn}^{13} &= a_{mnmn}^{31} = - \left\{ D_{22} \left(\frac{\pi}{b} \right)^3 \left[(1+n^2)^2 + 4n^2 \right] + (D_{12} + 2D_{66}) \left(\frac{\pi}{a} \right)^2 \left(\frac{\pi}{b} \right) (1+m^2)(1+n^2) \right\} \quad (\text{B-6}) \\
a_{mnmn}^{22} &= D_{11} \left(\frac{\pi}{a} \right)^2 \left[(1+m^2)^2 + 4m^2 \right] + D_{66} \left(\frac{\pi}{b} \right)^2 (1+m^2)(1+n^2) + D_{Qx} (1+m^2) \\
a_{mnmn}^{23} &= a_{mnmn}^{32} = (D_{12} + D_{66}) \left(\frac{\pi}{a} \right) \left(\frac{\pi}{b} \right) (1+m^2)(1+n^2) \\
a_{mnmn}^{33} &= D_{22} \left(\frac{\pi}{b} \right)^2 \left[(1+n^2)^2 + 4n^2 \right] + 2D_{66} \left(\frac{\pi}{a} \right)^2 (1+m^2)(1+n^2) + D_{Qy} (1+n^2)
\end{aligned}$$

5. $m = k = 1, n - l = 2$

$$\begin{aligned}
a_{1n1l}^{11} &= - \left[4D_{11} \left(\frac{\pi}{a} \right)^4 + 2(D_{12} + 2D_{66}) \left(\frac{\pi}{a} \right)^2 \left(\frac{\pi}{b} \right)^2 (1+l)^2 + \frac{3}{4} D_{22} \left(\frac{\pi}{b} \right)^4 (1+l)^4 \right] \\
a_{1n1l}^{12} &= a_{1n1l}^{21} = 4D_{11} \left(\frac{\pi}{a} \right)^3 + (D_{12} + 2D_{66}) \left(\frac{\pi}{a} \right) \left(\frac{\pi}{b} \right)^2 (1+l)^2 \\
a_{1n1l}^{13} &= a_{1n1l}^{31} = \frac{3}{4} D_{22} \left(\frac{\pi}{b} \right)^3 (1+l)^4 + (D_{12} + 2D_{66}) \left(\frac{\pi}{a} \right)^2 \left(\frac{\pi}{b} \right) (1+l)^2 \quad (\text{B-7}) \\
a_{1n1l}^{22} &= - \left[4D_{11} \left(\frac{\pi}{a} \right)^2 + D_{66} \left(\frac{\pi}{b} \right)^2 (1+l)^2 + D_{Qx} \right] \\
a_{1n1l}^{23} &= a_{1n1l}^{32} = -(D_{12} + D_{66}) \left(\frac{\pi}{a} \right) \left(\frac{\pi}{b} \right) (1+l)^2
\end{aligned}$$

6. $m = k \neq 1, n - l = 2$

$$\begin{aligned}
a_{mnml}^{11} &= - \frac{1}{2} \left\{ D_{11} \left(\frac{\pi}{4} \right)^4 \left[(1+m^2)^2 + 4m^2 \right] + 2(D_{12} + 2D_{66}) \left(\frac{\pi}{a} \right)^2 \left(\frac{\pi}{b} \right)^2 (1+m^2)(1+l)^2 + D_{22} \left(\frac{\pi}{b} \right)^4 (1+l)^4 \right\} \\
a_{mnml}^{12} &= a_{mnml}^{21} = \frac{1}{2} \left\{ D_{11} \left(\frac{\pi}{a} \right)^3 \left[(1+m^2)^2 + 4m^2 \right] + (D_{12} + 2D_{66}) \left(\frac{\pi}{a} \right) \left(\frac{\pi}{b} \right)^2 (1+m^2)(1+l)^2 \right\} \\
a_{mnml}^{13} &= a_{mnml}^{31} = \frac{1}{2} \left\{ D_{22} \left(\frac{\pi}{b} \right)^3 (1+l)^4 + (D_{12} + 2D_{66}) \left(\frac{\pi}{a} \right)^2 \left(\frac{\pi}{b} \right) (1+m^2)(1+l)^2 \right\} \quad (\text{B-8})
\end{aligned}$$

$$a_{mnml}^{22} = -\frac{1}{2} \left\{ D_{11} \left(\frac{\pi}{a} \right)^2 \left[(1+m^2)^2 + 4m^2 \right] + D_{66} \left(\frac{\pi}{b} \right)^2 (1+m^2)(1+l)^2 + D_{Qx} (1+m^2) \right\}$$

$$a_{mnml}^{23} = a_{mnml}^{32} = -\frac{1}{2} (D_{12} + D_{66}) \left(\frac{\pi}{a} \right) \left(\frac{\pi}{b} \right) (1+m^2)(1+l)^2$$

$$a_{mnml}^{33} = -\frac{1}{2} \left[D_{22} \left(\frac{\pi}{b} \right)^2 (1+l)^4 + D_{66} \left(\frac{\pi}{a} \right)^2 (1+m^2)(1+l)^2 + D_{Qy} (1+l)^2 \right]$$

7. $m-k=2, n=l=1$

$$\begin{aligned} a_{m1k1}^{11} &= -\left[\frac{3}{4} D_{11} \left(\frac{\pi}{a} \right)^4 (1+k)^4 + 2(D_{12} + 2D_{66}) \left(\frac{\pi}{a} \right)^2 \left(\frac{\pi}{b} \right)^2 (1+k)^2 + 4D_{22} \left(\frac{\pi}{b} \right)^4 \right] \\ a_{m1k1}^{12} &= a_{m1k1}^{21} = \frac{3}{4} D_{11} \left(\frac{\pi}{a} \right)^3 (1+k)^4 + (D_{12} + 2D_{66}) \left(\frac{\pi}{a} \right) \left(\frac{\pi}{b} \right)^2 (1+k)^2 \\ a_{m1k1}^{13} &= a_{m1k1}^{31} = 4D_{22} \left(\frac{\pi}{b} \right)^3 + (D_{12} + 2D_{66}) \left(\frac{\pi}{a} \right)^2 \left(\frac{\pi}{b} \right) (1+k)^2 \\ a_{m1k1}^{22} &= -\left[\frac{3}{4} D_{11} \left(\frac{\pi}{a} \right)^2 (1+k)^4 + D_{66} \left(\frac{\pi}{b} \right)^2 (1+k)^2 + \frac{3}{4} D_{Qx} (1+k)^2 \right] \\ a_{m1k1}^{23} &= a_{m1k1}^{32} = -(D_{12} + D_{66}) \left(\frac{\pi}{a} \right) \left(\frac{\pi}{b} \right) (1+k)^2 \\ a_{m1k1}^{33} &= -\left[4D_{22} \left(\frac{\pi}{b} \right)^2 + D_{66} \left(\frac{\pi}{a} \right)^2 (1+k)^2 + D_{Qy} \right] \end{aligned} \tag{B-9}$$

8. $m-k=2, n = l \neq 1$

$$\begin{aligned} a_{mnkn}^{11} &= -\frac{1}{2} \left\{ D_{11} \left(\frac{\pi}{a} \right)^4 (1+k)^4 + 2(D_{12} + 2D_{66}) \left(\frac{\pi}{a} \right)^2 \left(\frac{\pi}{b} \right)^2 (1+k)^2 (1+n^2) + D_{22} \left(\frac{\pi}{b} \right)^4 \left[(1+n^2)^2 + 4n^2 \right] \right\} \\ a_{mnkn}^{12} &= a_{mnkn}^{21} = \frac{1}{2} \left[D_{11} \left(\frac{\pi}{a} \right)^3 (1+k)^4 + (D_{12} + 2D_{66}) \left(\frac{\pi}{a} \right) \left(\frac{\pi}{b} \right)^2 (1+k)^2 (1+n^2) \right] \\ a_{mnkn}^{13} &= a_{mnkn}^{31} = \frac{1}{2} \left[D_{22} \left(\frac{\pi}{b} \right)^3 \left[(1+n^2)^2 + 4n^2 \right] + (D_{12} + 2D_{66}) \left(\frac{\pi}{a} \right)^2 \left(\frac{\pi}{b} \right) (1+k)^2 (1+n^2) \right] \\ a_{mnkn}^{22} &= -\frac{1}{2} \left[D_{11} \left(\frac{\pi}{a} \right)^2 (1+k)^4 + D_{66} \left(\frac{\pi}{b} \right)^2 (1+k)^2 (1+n^2) + D_{Qx} (1+k)^2 \right] \\ a_{mnkn}^{23} &= a_{mnkn}^{32} = -\frac{1}{2} (D_{12} + D_{66}) \left(\frac{\pi}{a} \right) \left(\frac{\pi}{b} \right) (1+k)^2 (1+n^2) \\ a_{mnkn}^{33} &= -\frac{1}{2} \left\{ D_{22} \left(\frac{\pi}{b} \right)^2 \left[(1+n^2)^2 + 4n^2 \right] + D_{66} \left(\frac{\pi}{a} \right)^2 (1+k)^2 (1+n^2) + D_{Qy} (1+n^2) \right\} \end{aligned} \tag{B-10}$$

9. $m - k = 2, n - l = 2$

$$\begin{aligned}
 a_{mnkl}^{11} &= \frac{1}{4} \left[D_{11} \left(\frac{\pi}{a} \right)^4 (1+k)^4 + 2(D_{12} + 2D_{66}) \left(\frac{\pi}{a} \right)^2 \left(\frac{\pi}{b} \right)^2 (1+k)^2 (1+l)^2 + D_{22} \left(\frac{\pi}{b} \right)^4 (1+l)^4 \right] \\
 a_{mnkl}^{12} &= a_{mnkl}^{21} = -\frac{1}{4} \left[D_{11} \left(\frac{\pi}{a} \right)^3 (1+k)^4 + (D_{12} + 2D_{66}) \left(\frac{\pi}{a} \right)^2 \left(\frac{\pi}{b} \right)^2 (1+k)^2 (1+l)^2 \right] \\
 a_{mnkl}^{13} &= a_{mnkl}^{31} = -\frac{1}{4} \left[D_{22} \left(\frac{\pi}{b} \right)^3 (1+l)^4 + (D_{12} + 2D_{66}) \left(\frac{\pi}{a} \right)^2 \left(\frac{\pi}{b} \right) (1+k)^2 (1+l)^2 \right] \tag{B-11} \\
 a_{mnkl}^{22} &= \frac{1}{4} \left[D_{11} \left(\frac{\pi}{a} \right)^2 (1+k)^4 + D_{66} \left(\frac{\pi}{b} \right)^2 (1+k)^2 (1+l)^2 + D_{Qx} (1+k)^2 \right] \\
 a_{mnkl}^{23} &= a_{mnkl}^{32} = \frac{1}{4} (D_{12} + D_{66}) \left(\frac{\pi}{a} \right) \left(\frac{\pi}{b} \right) (1+k)^2 (1+l)^2 \\
 a_{mnkl}^{33} &= \frac{1}{4} \left[D_{22} \left(\frac{\pi}{b} \right)^2 (1+l)^4 + D_{66} \left(\frac{\pi}{a} \right)^2 (1+k)^2 (1+l)^2 + D_{Qy} (1+l)^2 \right]
 \end{aligned}$$

APPENDIX C TABLE OF SPECIAL INTEGRALS

Different types of integrals are needed to carry out the integration of strain energy expression associated with the dome-shaped temperature profile heating.

Special Integrals Needed for 4S Case:

$$\int_0^a \cos \frac{m\pi x}{a} \cos \frac{k\pi x}{a} dx = \frac{a}{2} ; \quad m = k$$

$$\int_0^b \cos \frac{n\pi y}{b} \cos \frac{l\pi y}{b} dy = \frac{b}{2} ; \quad n = l$$

$$\int_0^a \sin \frac{m\pi x}{a} \sin \frac{k\pi x}{a} \sin \frac{\pi x}{a} dx = -\frac{4a}{\pi} \frac{mk}{[(m+k)^2 - 1][(m-k)^2 - 1]} ; \quad m \pm k = \text{even}$$

$$\int_0^b \sin \frac{n\pi y}{b} \sin \frac{l\pi y}{b} \sin \frac{\pi y}{b} dy = -\frac{4b}{\pi} \frac{nl}{[(n+l)^2 - 1][(n-l)^2 - 1]} ; \quad n \pm l = \text{even}$$

Special Integrals Needed for 4C Case:

$$\int_0^a \sin \frac{\pi x}{a} \cos^2 \frac{\pi x}{a} \sin \frac{m\pi x}{a} \sin \frac{k\pi x}{a} dx = -\frac{amk}{\pi} \left\{ \frac{1}{[(m+k)^2 - 1][(m-k)^2 - 1]} + \frac{3}{[(m+k)^2 - 9][(m-k)^2 - 9]} \right\}$$

$$m \pm k = \text{even}$$

$$\int_0^a \sin^2 \frac{\pi x}{a} \cos \frac{\pi x}{a} \sin \frac{m\pi x}{a} \cos \frac{k\pi x}{a} dx = \frac{am}{2\pi} \left\{ \frac{(m^2 - k^2) - 1}{[(m+k)^2 - 1][(m-k)^2 - 1]} - \frac{(m^2 - k^2) - 9}{[(m+k)^2 - 9][(m-k)^2 - 9]} \right\}$$

$$m \pm k = \text{even}$$

$$\int_0^a \sin^2 \frac{\pi x}{a} \cos \frac{\pi x}{a} \cos \frac{m\pi x}{a} \sin \frac{k\pi x}{a} dx = -\frac{ak}{2\pi} \left\{ \frac{(m^2 - k^2) + 1}{[(m+k)^2 - 1][(m-k)^2 - 1]} - \frac{(m^2 - k^2) + 9}{[(m+k)^2 - 9][(m-k)^2 - 9]} \right\}$$

$$m \pm k = \text{even}$$

$$\int_0^a \sin^3 \frac{\pi x}{a} \cos \frac{m\pi x}{a} \cos \frac{k\pi x}{a} dx = -\frac{3a}{2\pi} \left\{ \frac{(m^2 + k^2) - 1}{[(m+k)^2 - 1][(m-k)^2 - 1]} - \frac{(m^2 + k^2) - 9}{[(m+k)^2 - 9][(m-k)^2 - 9]} \right\}$$

$m \pm k = \text{even}$

$$\int_0^a \sin^3 \frac{\pi x}{a} \sin \frac{m\pi x}{a} \sin \frac{k\pi x}{a} dx = -\frac{3amk}{\pi} \left\{ \frac{1}{[(m+k)^2 - 1][(m-k)^2 - 1]} - \frac{1}{[(m+k)^2 - 9][(m-k)^2 - 9]} \right\}$$

$m \pm k = \text{even}$

$$\int_0^b \sin \frac{\pi y}{b} \cos^2 \frac{\pi y}{b} \sin \frac{n\pi y}{b} \sin \frac{l\pi y}{b} dy = -\frac{bnl}{\pi} \left\{ \frac{1}{[(n+l)^2 - 1][(n-l)^2 - 1]} + \frac{3}{[(n+l)^2 - 9][(n-l)^2 - 9]} \right\}$$

$n \pm l = \text{even}$

$$\int_0^b \sin^2 \frac{\pi y}{b} \cos \frac{\pi y}{b} \sin \frac{m\pi y}{b} \cos \frac{k\pi y}{b} dy = \frac{bn}{2\pi} \left\{ \frac{(n^2 - l^2) - 1}{[(n+l)^2 - 1][(n-l)^2 - 1]} - \frac{(n^2 - l^2) - 9}{[(n+l)^2 - 9][(n-l)^2 - 9]} \right\}$$

$n \pm l = \text{even}$

$$\int_0^b \sin^2 \frac{\pi y}{b} \cos \frac{\pi y}{b} \cos \frac{n\pi y}{b} \sin \frac{l\pi y}{b} dy = -\frac{bl}{2\pi} \left\{ \frac{(n^2 - l^2) + 1}{[(n+l)^2 - 1][(n-l)^2 - 1]} - \frac{(n^2 - l^2) + 9}{[(n+l)^2 - 9][(n-l)^2 - 9]} \right\}$$

$n \pm l = \text{even}$

$$\int_0^b \sin^3 \frac{\pi y}{b} \cos \frac{n\pi y}{b} \cos \frac{l\pi y}{b} dy = -\frac{3b}{2\pi} \left\{ \frac{(n^2 + l^2) - 1}{[(n+l)^2 - 1][(n-l)^2 - 1]} - \frac{(n^2 + l^2) - 9}{[(n+l)^2 - 9][(n-l)^2 - 9]} \right\}$$

$n \pm l = \text{even}$

$$\int_0^b \sin^3 \frac{\pi y}{b} \sin \frac{n\pi y}{b} \sin \frac{l\pi y}{b} dy = -\frac{3bnl}{\pi} \left\{ \frac{1}{[(n+l)^2 - 1][(n-l)^2 - 1]} - \frac{1}{[(n+l)^2 - 9][(n-l)^2 - 9]} \right\}$$

$n \pm l = \text{even}$

APPENDIX D

BUCKLING EQUATIONS

Case 1: 4S condition

$m \pm n = \text{even}$ (symmetric buckling)

$A_{kl} \rightarrow$	A_{11}	A_{13}	A_{22}	A_{31}	A_{15}	A_{24}	A_{33}	A_{42}	A_{51}	A_{35}	A_{44}	A_{53}	
$m=1, n=1$	$\frac{M_{1111}}{T_o} + P_{1111}$	P_{1113}	0	P_{1131}	P_{1115}	0	P_{1133}	0	P_{1151}	P_{1135}	0	P_{1153}	
$m=1, n=3$		$\frac{M_{1313}}{T_o} + P_{1313}$	0	P_{1331}	P_{1315}	0	P_{1333}	0	P_{1351}	P_{1335}	0	P_{1353}	
$m=2, n=2$		$\frac{M_{2222}}{T_o} + P_{2222}$	0	0	P_{2224}	0	P_{2242}	0	0	P_{2244}	0		
$m=3, n=1$			$\frac{M_{3131}}{T_o} + P_{3131}$	P_{3115}	0	P_{3133}	0	P_{3151}	P_{3135}	0	P_{3133}		
$m=1, n=5$				$\frac{M_{1515}}{T_o} + P_{1515}$	0	P_{1533}	0	P_{1551}	P_{1535}	0	P_{1553}		
$m=2, n=4$					$\frac{M_{2424}}{T_o} + P_{2424}$	0	P_{2442}	0	0	P_{2444}	0		$= 0$
$m=3, n=3$						$\frac{M_{3333}}{T_o} + P_{3333}$	0	P_{3351}	P_{3335}	0	P_{3353}		
$m=4, n=2$		Symmetry					$\frac{M_{4242}}{T_o} + P_{4242}$	0	0	P_{4244}	0		
$m=5, n=1$								$\frac{M_{5151}}{T_o} + P_{5151}$	P_{5135}	0	P_{5153}		
$m=3, n=5$									$\frac{M_{3535}}{T_o} + P_{3535}$	0	P_{3553}		
$m=4, n=4$										$\frac{M_{4444}}{T_o} + P_{4444}$	0		
$m=5, n=3$											$\frac{M_{5353}}{T_o} + P_{5353}$		

(D-1)

Case 1: 4S condition

 $m \pm n = \text{odd}$ (antisymmetric buckling)

$A_{kl} \rightarrow$	A_{12}	A_{21}	A_{14}	A_{23}	A_{32}	A_{41}	A_{16}	A_{25}	A_{34}	A_{43}	A_{52}	A_{61}	
$m=1, n=2$	$\frac{M_{1212}}{T_o} + P_{1212}$	0	P_{1214}	0	P_{1232}	0	P_{1216}	0	P_{1234}	0	P_{1252}	0	
$m=2, n=1$		$\frac{M_{2121}}{T_o} + P_{2121}$	0	P_{2123}	0	P_{2141}	0	P_{2125}	0	P_{2143}	0	P_{2161}	
$m=1, n=4$			$\frac{M_{1414}}{T_o} + P_{1414}$	0	P_{1432}	0	P_{1416}	0	P_{1434}	0	P_{1452}	0	
$m=2, n=3$				$\frac{M_{2323}}{T_o} + P_{2323}$	0	P_{2341}	0	P_{2325}	0	P_{2343}	0	P_{2361}	
$m=3, n=2$					$\frac{M_{3232}}{T_o} + P_{3232}$	0	P_{3216}	0	P_{3234}	0	P_{3252}	0	
$m=4, n=1$						$\frac{M_{4141}}{T_o} + P_{4141}$	0	P_{4125}	0	P_{4143}	0	P_{4161}	= 0
$m=1, n=6$							$\frac{M_{1616}}{T_o} + P_{1616}$	0	P_{1634}	0	P_{1652}	0	
$m=2, n=5$	Symmetry							$\frac{M_{2525}}{T_o} + P_{2525}$	0	P_{2543}	0	P_{2561}	
$m=3, n=4$									$\frac{M_{3434}}{T_o} + P_{3434}$	0	P_{3452}	0	
$m=4, n=3$										$\frac{M_{4343}}{T_o} + P_{4343}$	0	P_{4361}	
$m=5, n=2$											$\frac{M_{5252}}{T_o} + P_{5252}$	0	
$m=6, n=1$												$\frac{M_{6161}}{T_o} + P_{6161}$	

(D-2)

Case 2: 4C condition

$m \pm n = \text{even}$ (symmetric buckling)

$A_{kl} \rightarrow$	A_{11}	A_{13}	A_{22}	A_{31}	A_{15}	A_{24}	A_{33}	A_{42}	A_{51}	A_{35}	A_{44}	A_{53}
$m=1, n=1$	$\frac{M_{1111}}{T_o} + P_{1111}$	$\frac{M_{1113}}{T_o} + P_{1113}$	0	$\frac{M_{1131}}{T_o} + P_{1131}$	P_{1115}	0	$\frac{M_{1133}}{T_o} + P_{1133}$	0	P_{1151}	P_{1135}	0	P_{1153}
$m=1, n=3$		$\frac{M_{1313}}{T_o} + P_{1313}$	0	$\frac{M_{1331}}{T_o} + P_{1331}$	$\frac{M_{1315}}{T_o} + P_{1315}$	0	$\frac{M_{1333}}{T_o} + P_{1333}$	0	P_{1351}	$\frac{M_{1335}}{T_o} + P_{1335}$	0	P_{1353}
$m=2, n=2$		$\frac{M_{2222}}{T_o} + P_{2222}$	0	0	$\frac{M_{2224}}{T_o} + P_{2224}$	0	$\frac{M_{2242}}{T_o} + P_{2242}$	0	0	$\frac{M_{2244}}{T_o} + P_{2244}$	0	
$m=3, n=1$			$\frac{M_{3131}}{T_o} + P_{3131}$	P_{3115}	0	$\frac{M_{3133}}{T_o} + P_{3133}$	0	$\frac{M_{3151}}{T_o} + P_{3151}$	P_{3135}	0	$\frac{M_{3153}}{T_o} + P_{3153}$	
$m=1, n=5$				$\frac{M_{1515}}{T_o} + P_{1515}$	0	$\frac{M_{1533}}{T_o} + P_{1533}$	0	P_{1551}	$\frac{M_{1535}}{T_o} + P_{1535}$	0	P_{1553}	
$m=2, n=4$					$\frac{M_{2424}}{T_o} + P_{2424}$	0	$\frac{M_{2442}}{T_o} + P_{2442}$	0	0	$\frac{M_{2444}}{T_o} + P_{2444}$	$\frac{M_{2453}}{T_o} + P_{2453}$	= 0
$m=3, n=3$						$\frac{M_{3333}}{T_o} + P_{3333}$	0	$\frac{M_{3351}}{T_o} + P_{3351}$	$\frac{M_{3335}}{T_o} + P_{3335}$	0	$\frac{M_{3353}}{T_o} + P_{3353}$	
$m=4, n=2$	Symmetry						$\frac{M_{4242}}{T_o} + P_{4242}$	0	0	$\frac{M_{4244}}{T_o} + P_{4244}$	0	
$m=5, n=1$								$\frac{M_{5151}}{T_o} + P_{5151}$	P_{5135}	0	$\frac{M_{5153}}{T_o} + P_{5153}$	
$m=3, n=5$									$\frac{M_{3535}}{T_o} + P_{3535}$	0	$\frac{M_{3553}}{T_o} + P_{3553}$	
$m=4, n=4$										$\frac{M_{4444}}{T_o} + P_{4444}$	0	
$m=5, n=3$											$\frac{M_{5353}}{T_o} + P_{5353}$	

(D-3)

Case 2: 4C condition

 $m \pm n = \text{odd}$ (antisymmetric buckling)

$$\begin{array}{c|cccccccccccc}
A_{kl} \rightarrow & A_{12} & A_{21} & A_{14} & A_{23} & A_{32} & A_{41} & A_{16} & A_{25} & A_{34} & A_{43} & A_{52} & A_{61} \\
\hline
m=1, n=2 & \frac{M_{1212}}{T_o} + P_{1212} & 0 & \frac{M_{1214}}{T_o} + P_{1214} & 0 & \frac{M_{1232}}{T_o} + P_{1232} & 0 & P_{1216} & 0 & \frac{M_{1234}}{T_o} + P_{1234} & 0 & P_{1252} & 0 \\
m=2, n=1 & \frac{M_{2121}}{T_o} + P_{2121} & 0 & \frac{M_{2123}}{T_o} + P_{2123} & 0 & \frac{M_{2141}}{T_o} + P_{2141} & 0 & P_{2125} & 0 & \frac{M_{2143}}{T_o} + P_{2143} & 0 & P_{2161} \\
m=1, n=4 & \frac{M_{1414}}{T_o} + P_{1414} & 0 & \frac{M_{1432}}{T_o} + P_{1432} & 0 & \frac{M_{1416}}{T_o} + P_{1416} & 0 & \frac{M_{1434}}{T_o} + P_{1434} & 0 & P_{1452} & 0 \\
m=2, n=3 & \frac{M_{2323}}{T_o} + P_{2323} & 0 & \frac{M_{2341}}{T_o} + P_{2341} & 0 & \frac{M_{2325}}{T_o} + P_{2325} & 0 & \frac{M_{2343}}{T_o} + P_{2343} & 0 & P_{2361} \\
m=3, n=2 & \frac{M_{3232}}{T_o} + P_{3232} & 0 & P_{3216} & 0 & \frac{M_{3234}}{T_o} + P_{3234} & 0 & \frac{M_{3252}}{T_o} + P_{3252} & 0 \\
m=4, n=1 & \frac{M_{4141}}{T_o} + P_{4141} & 0 & P_{4125} & 0 & \frac{M_{4143}}{T_o} + P_{4143} & 0 & \frac{M_{4161}}{T_o} + P_{4161} & 0 \\
m=1, n=6 & \frac{M_{1616}}{T_o} + P_{1616} & 0 & \frac{M_{1634}}{T_o} + P_{1634} & 0 & P_{1652} & 0 \\
m=2, n=5 & \text{Symmetry} & & \frac{M_{2525}}{T_o} + P_{2525} & 0 & \frac{M_{2543}}{T_o} + P_{2543} & 0 & P_{2561} \\
m=3, n=4 & & & \frac{M_{3434}}{T_o} + P_{3434} & 0 & \frac{M_{3452}}{T_o} + P_{3452} & 0 \\
m=4, n=3 & & & \frac{M_{4343}}{T_o} + P_{4343} & 0 & \frac{M_{4361}}{T_o} + P_{4361} \\
m=5, n=2 & & & \frac{M_{5252}}{T_o} + P_{5252} & 0 \\
m=6, n=1 & & & \frac{M_{6161}}{T_o} + P_{6161} \\
\end{array}
= 0$$

(D-4)

REFERENCES

1. Richards, W. Lance and Randolph C. Thompson, "Titanium Honeycomb Panel Testing," *Proceedings, Structural Testing Technology at High Temperature Conference*, Dayton, Ohio, Nov. 4–6, 1991, Society for Experimental Mechanics, Inc., 1992, pp. 116–132.
2. Ko, William L., Robert D. Quinn, and Leslie Gong, *Finite-Element Reentry Heat-Transfer Analysis of Space Shuttle Orbiter*, NASA TP-2657, 1986.
3. Ko, William L. and Leslie Gong, *Thermostructural Analysis of Unconventional Wing Structures of a Hyper-X Hypersonic Flight Research Vehicle for the Mach 7 Mission*, NASA/TP-2001-210398, 2001.
4. Ko, William L. and Raymond H. Jackson, "Combined Compressive and Shear Buckling Analysis of Hypersonic Aircraft Structural Sandwich Panels," AIAA Paper No. 92-2487-CP, 33rd AIAA/ASME/ASCE/AHS/ASC Structures, Structural Dynamics and Materials Conference, Dallas, Texas, April 13–15, 1992. Also published as NASA TM-4290, 1991.
5. Ko, William L., "Mechanical and Thermal Buckling Analysis of Sandwich Panels Under Different Edge Conditions," *Proc. 1st Pacific International Conference on Aerospace Science and Technology*, Tainan, Taiwan, Dec. 6–9, 1993.
6. Ko, William L. and Raymond H. Jackson, *Mechanical and Thermal Bucklings of Rectangular Sandwich Panels Under Different Edge Conditions*, NASA TM-4585, 1994.
7. Ko, William L., *Predictions of Thermal Buckling Strengths of Hypersonic Aircraft Sandwich Panels Using Minimum Potential Energy and Finite Element Methods*, NASA TM-4643, 1995.
8. Ko, William L. and Raymond H. Jackson, *Combined-Load Buckling Behavior of Metal-Matrix Composite Sandwich Panels Under Different Thermal Environments*, NASA TM-4321, 1991.
9. Ko, William L. and Raymond H. Jackson, "Compressive and Shear Buckling Analysis of Metal Matrix Composite Sandwich Panels Under Different Thermal Environments," *Composite Structures*, Vol. 25, 1993, pp. 227–239.
10. Ko, William L., *Thermostructural Behavior of a Hypersonic Aircraft Sandwich Panel Subjected to Heating on One Side*, NASA TM-4769, 1997.
11. Whetstone, W. D., *SPAR Structural Analysis System Reference Manual, System Level 13A*, Vol. 1, Program Execution, NASA CR-158970-1, 1978.
12. Ko, William L., *Mechanical- and Thermal-Buckling Behavior of Rectangular Plates With Different Central Cutouts*, NASA/TM-1998-206542, 1998.

FIGURES

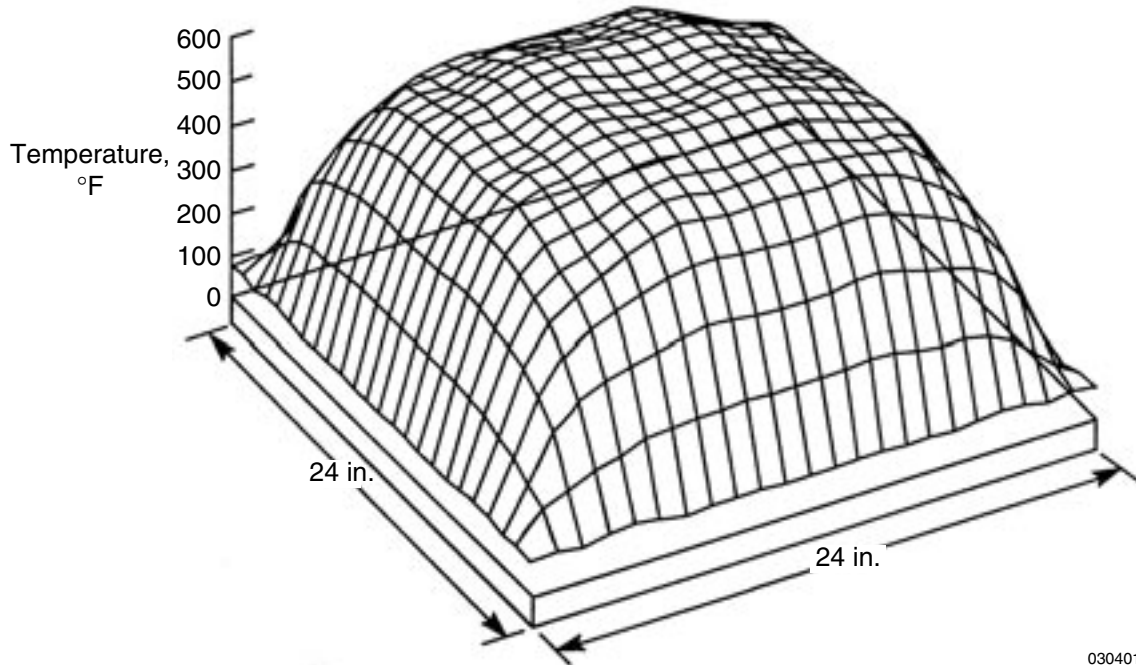


Figure 1. Measured temperature distribution in upper surface of titanium honeycomb-core sandwich panel, heated on upper side at 10°F/sec heating rate, with four edges supported by test fixtures (heat sink) (ref. 1).

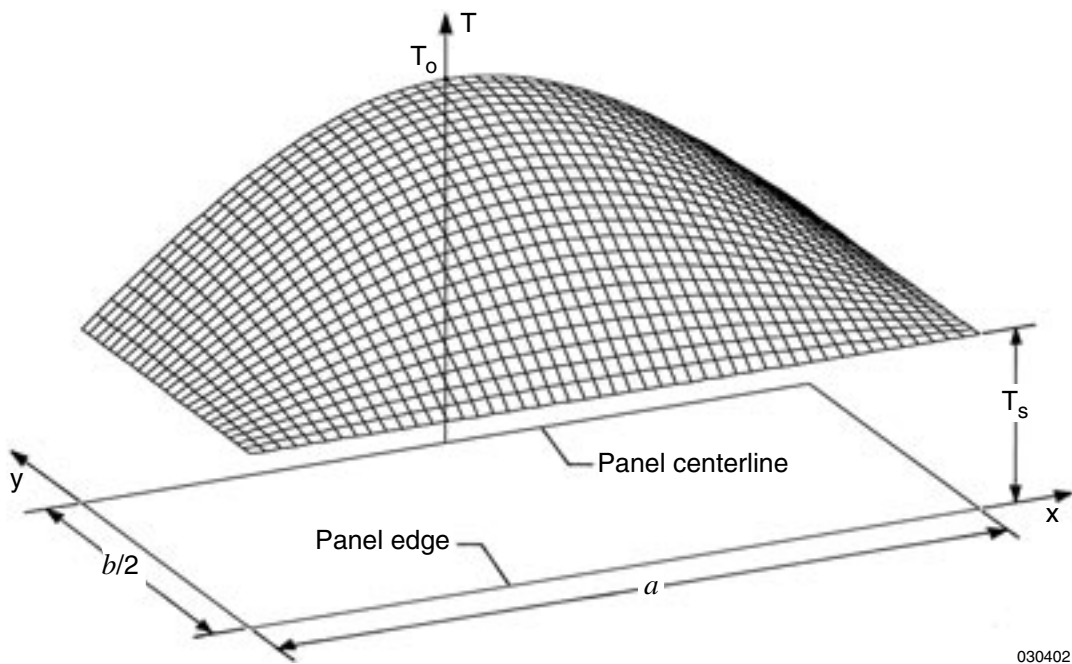


Figure 2. Shifted dome-shaped temperature profile heating ($T_s \neq 0$).

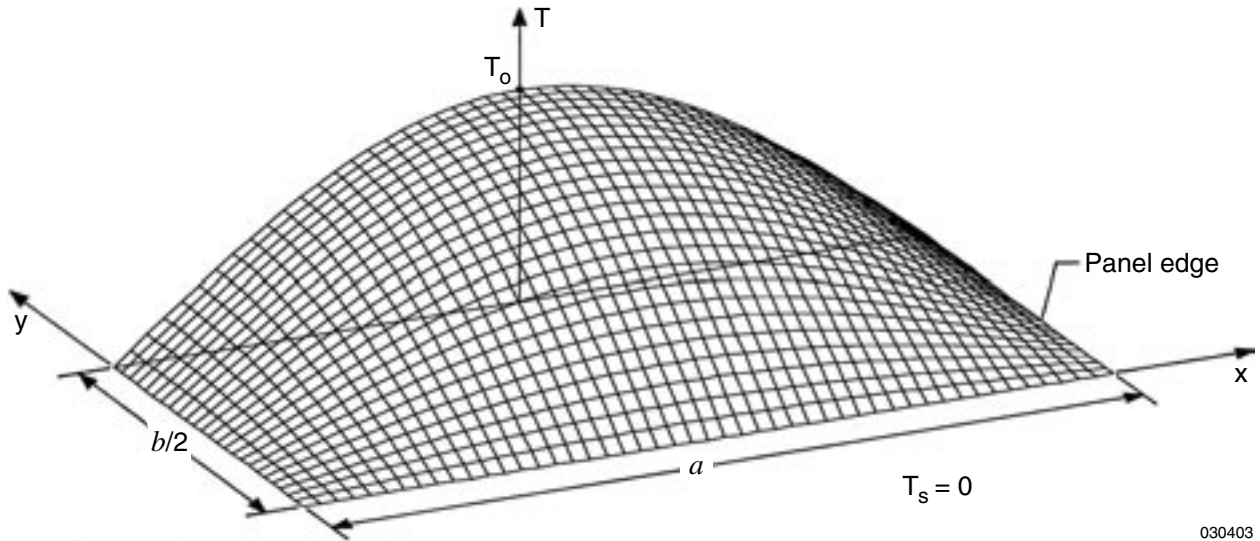


Figure 3. Dome-shaped temperature profile heating ($T_s = 0$).

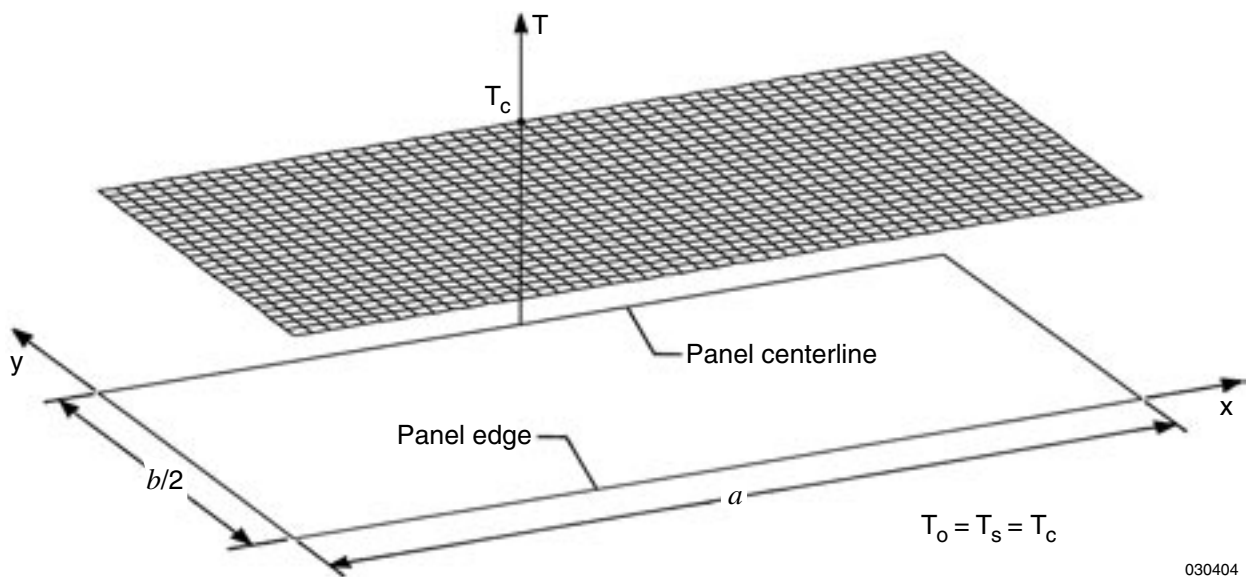


Figure 4. Uniform temperature profile heating ($T_o = T_s = T_c = \text{constant}$).

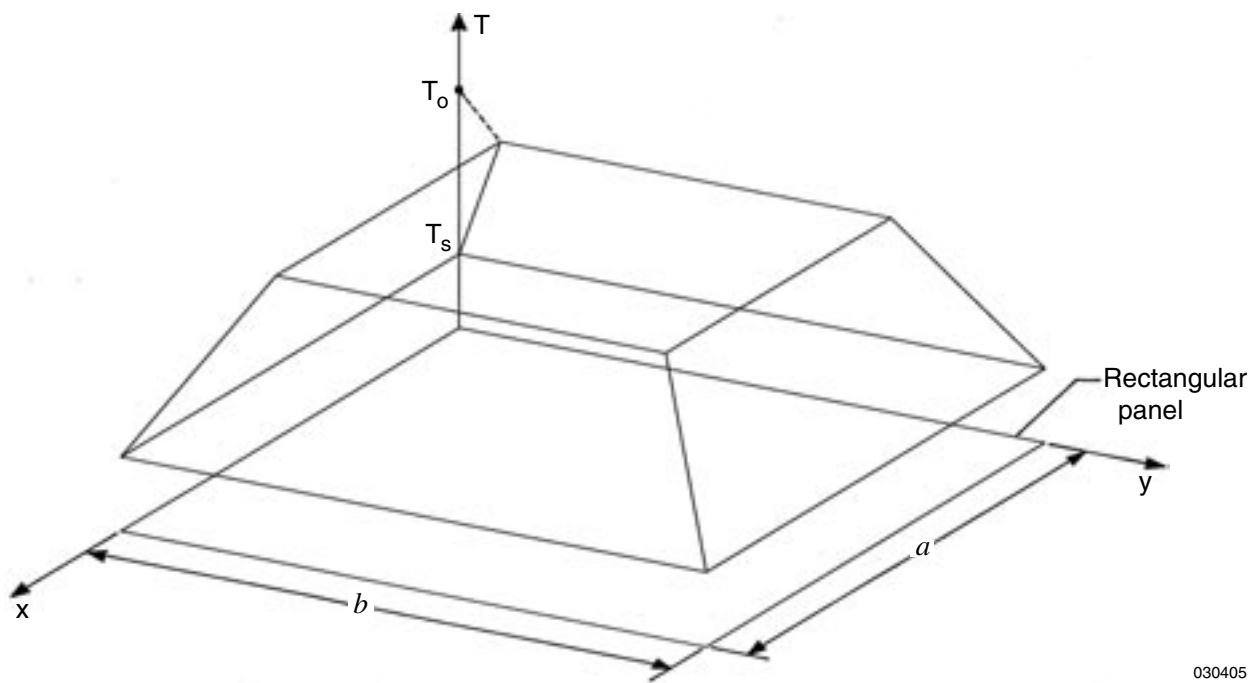


Figure 5. Shifted roof-shaped temperature profile heating ($T_s \neq 0$).

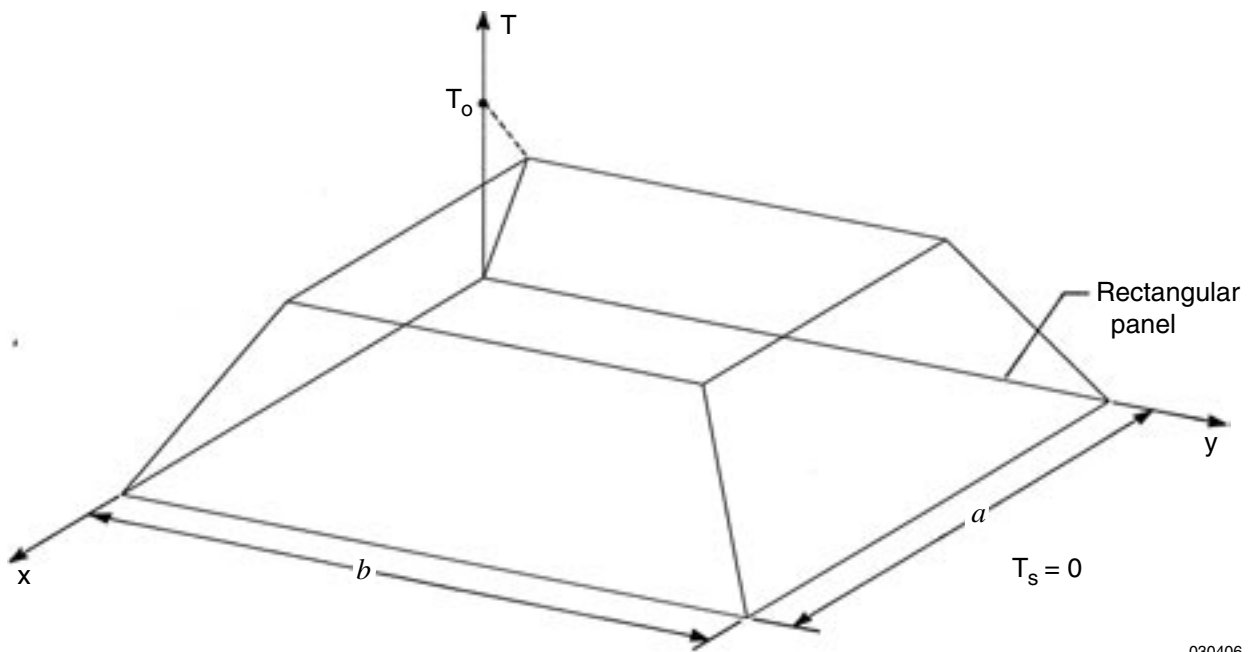


Figure 6. Roof-shaped temperature profile heating ($T_s = 0$).

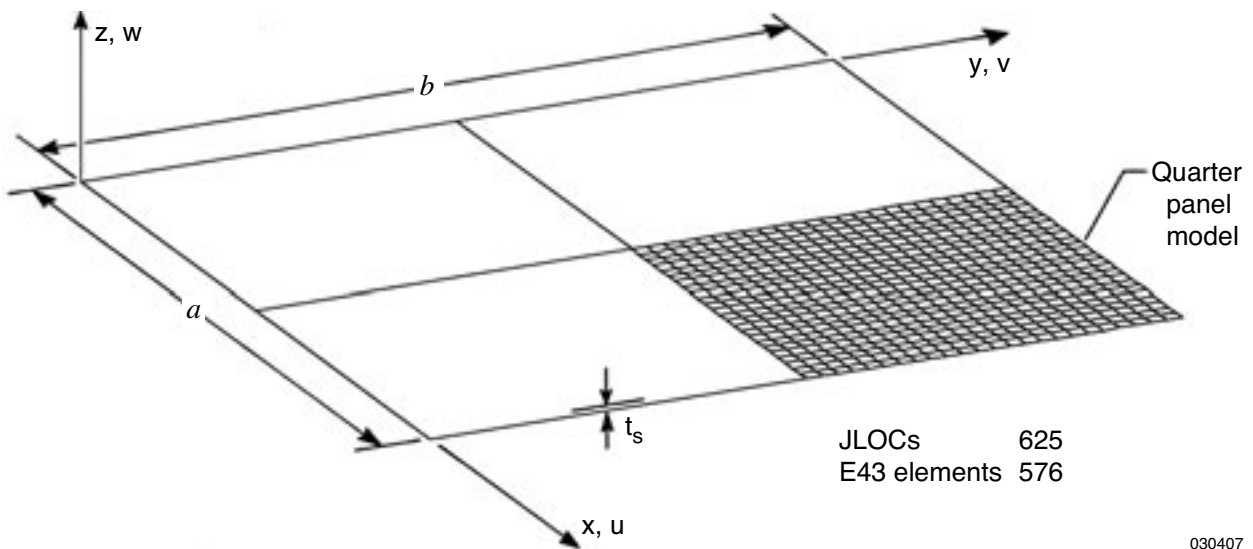
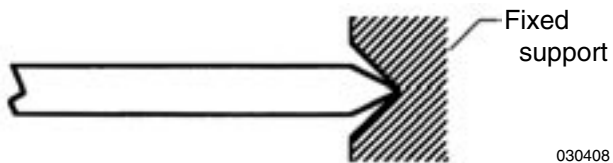
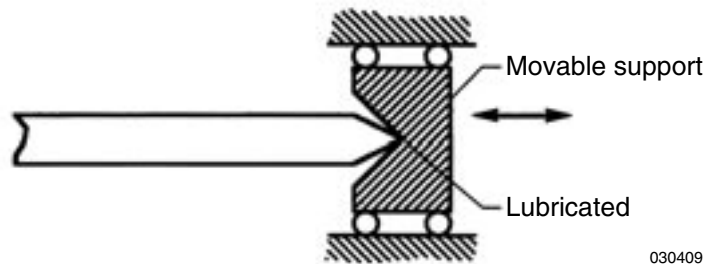


Figure 7. Quarter panel finite-element model for rectangular panel.

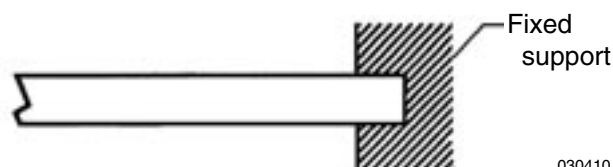


(a) 4S fixed.

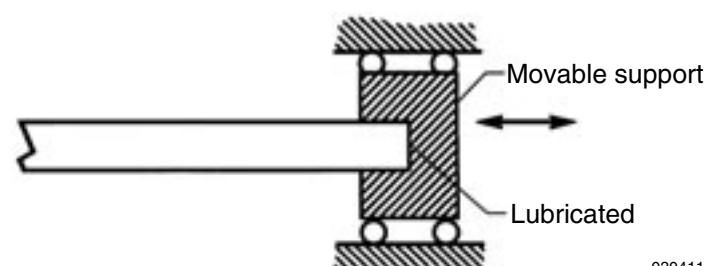


(b) 4S free.

Figure 8. Two types of boundary conditions for simply-supported edges.

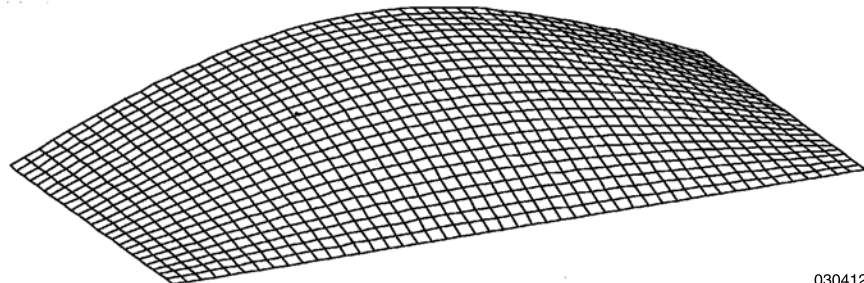


(a) 4C fixed.



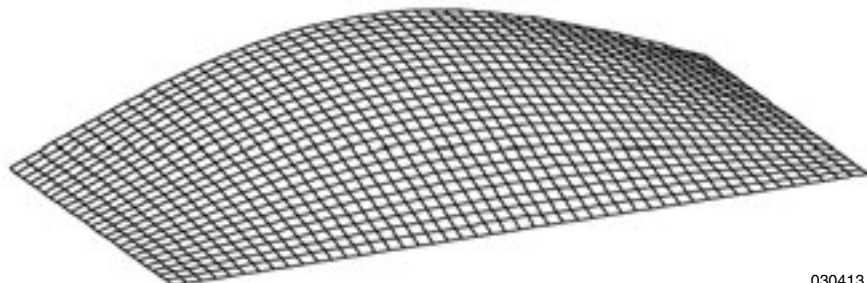
(b) 4C free.

Figure 9. Two types of boundary conditions for clamped edges.



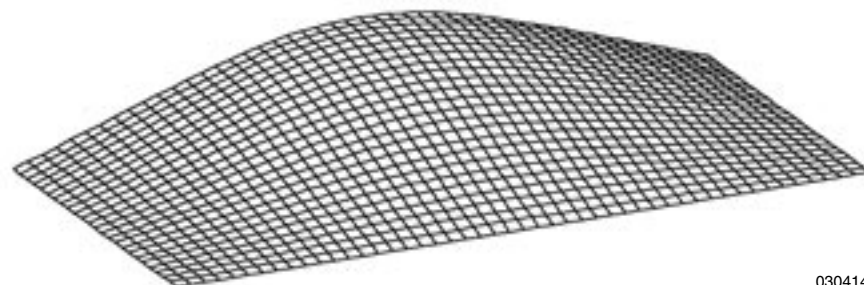
030412

(a) Uniform temperature profile heating.



030413

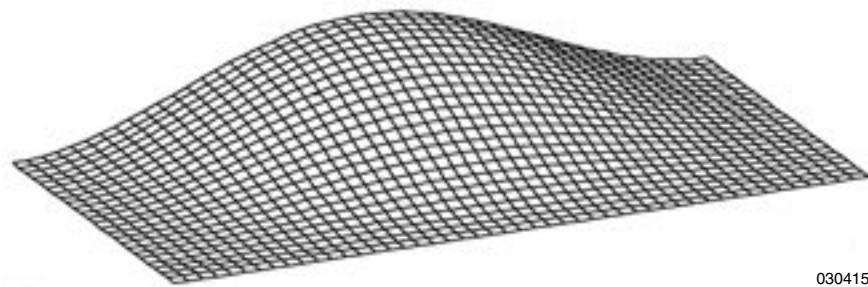
(b) Dome-shaped temperature profile heating.



030414

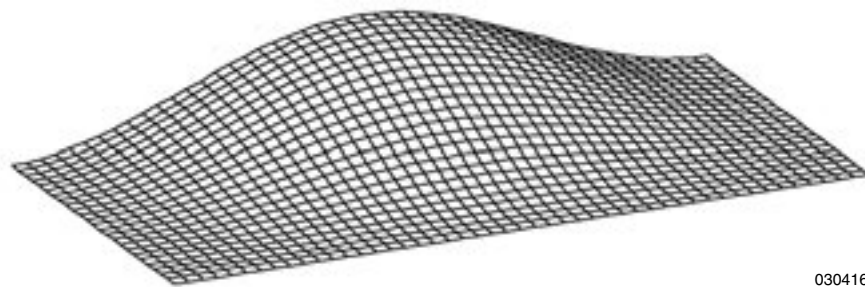
(c) Roof-shaped temperature profile heating.

Figure 10. Buckled shapes of square panel ($a/b = 1$) under different temperature profile heating; 4S fixed edge support conditions; $T_s = 0$.



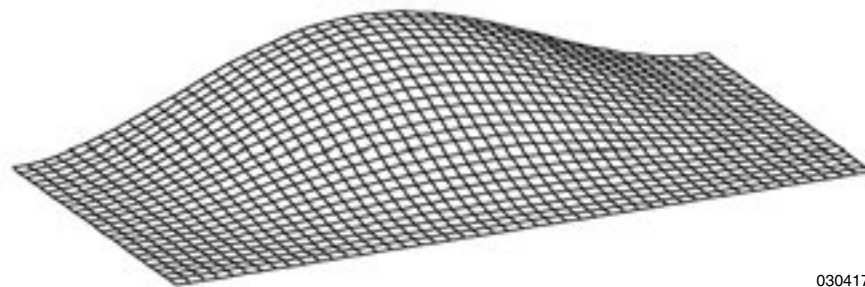
030415

(a) Uniform temperature profile heating.



030416

(b) Dome-shaped temperature profile heating.



030417

(c) Roof-shaped temperature profile heating.

Figure 11. Buckled shapes of square panel ($a/b = 1$) under different temperature profile heating; 4C fixed edge support conditions; $T_s = 0$.

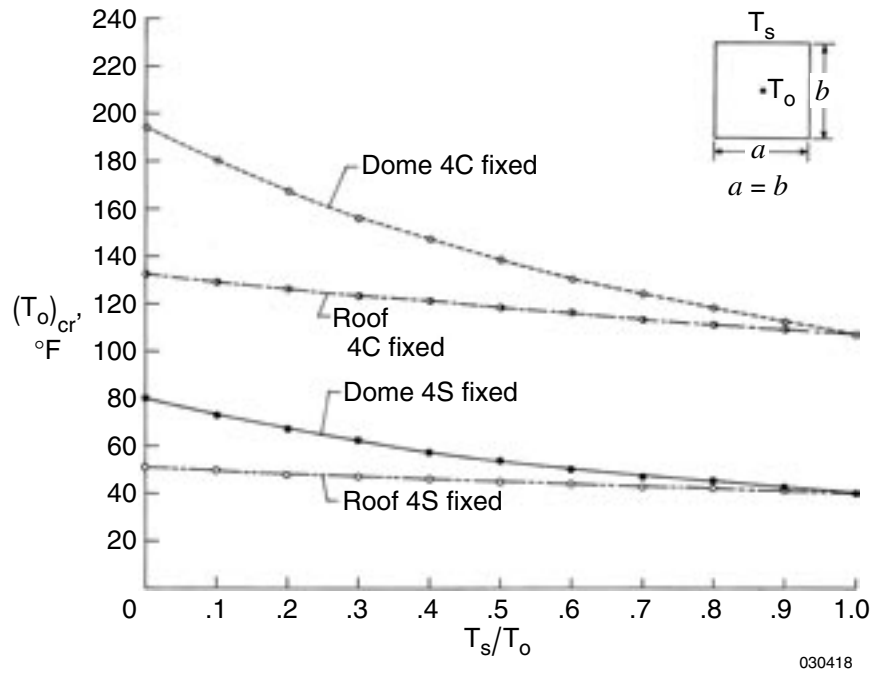


Figure 12. Plots of buckling temperatures $(T_o)_{cr}$ as functions of boundary heat sink temperature T_s/T_o for different temperature profile heating; fixed cases.

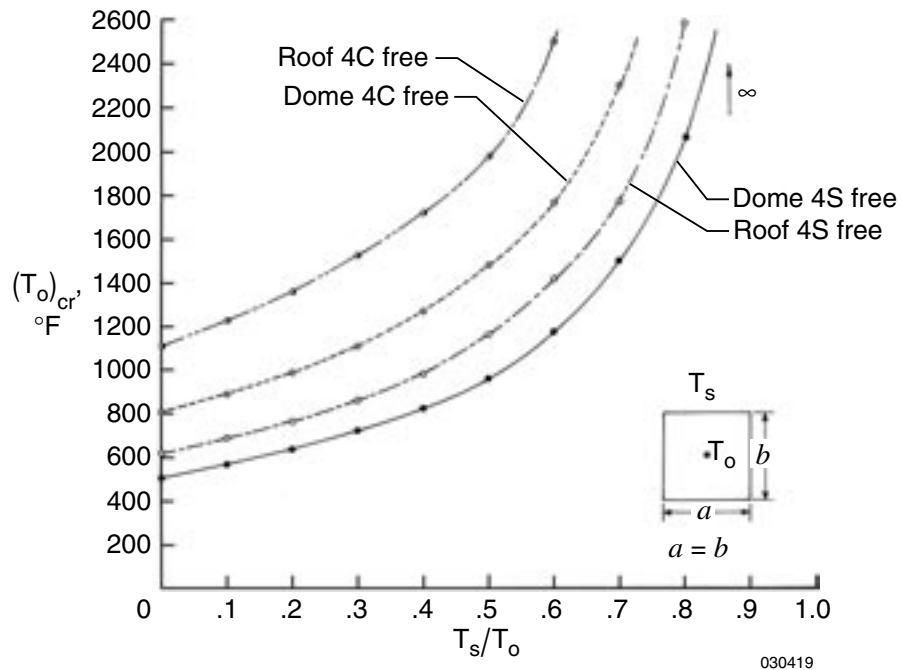


Figure 13. Plots of buckling temperatures $(T_o)_{cr}$ as functions of boundary heat sink temperature T_s/T_o for different temperature profile heating; free cases.

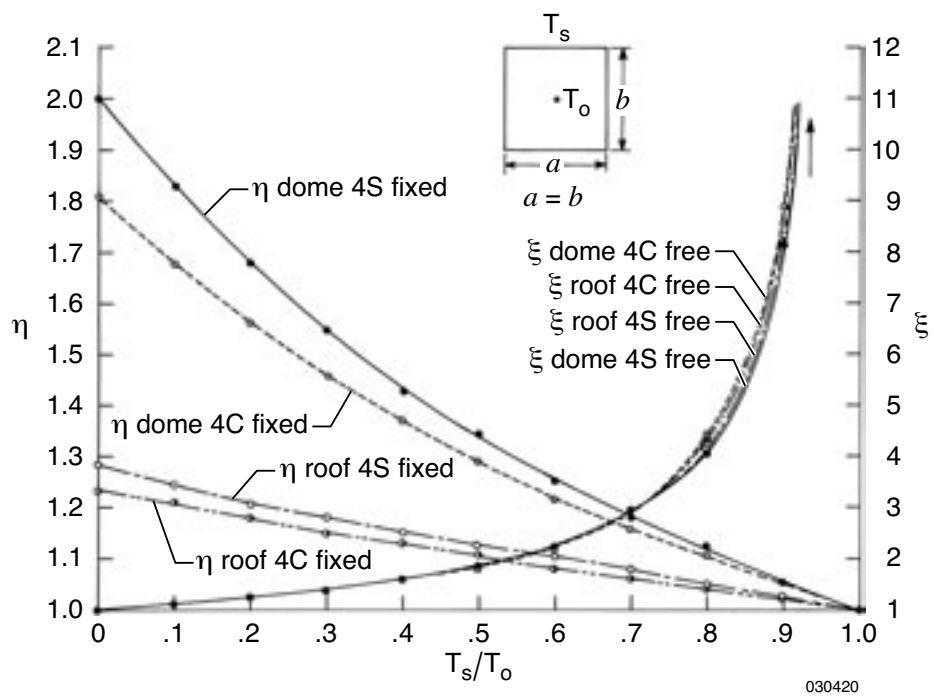
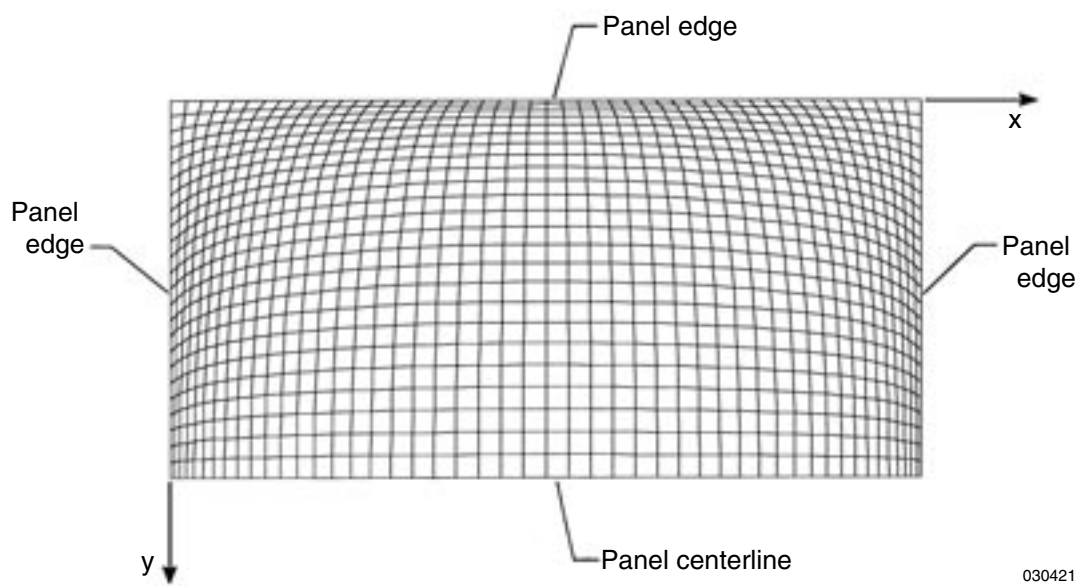
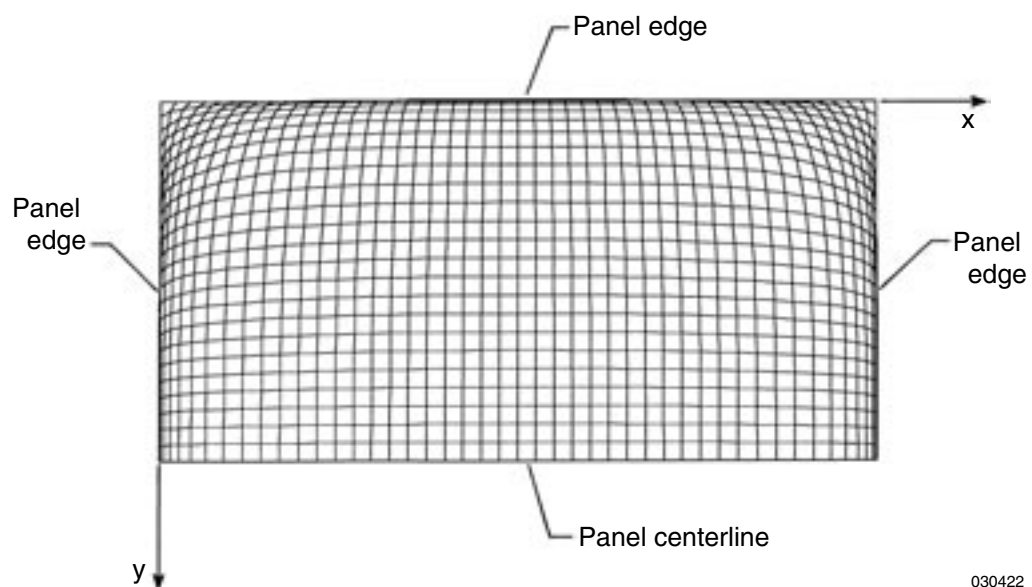


Figure 14. Plots of buckling temperature magnification factors of the first and the second kinds $\{\eta, \xi\}$ as functions of boundary heat sink temperature T_s/T_o .



(a) Dome-shaped temperature profile heating.



(b) Roof-shaped temperature profile heating.

Figure. 15. In-plane deformed shape of square panel under different temperature profile heating; four edges fixed; $u(x, y) \neq 0, v(x, y) \neq 0$ at panel interior; half panel plot.

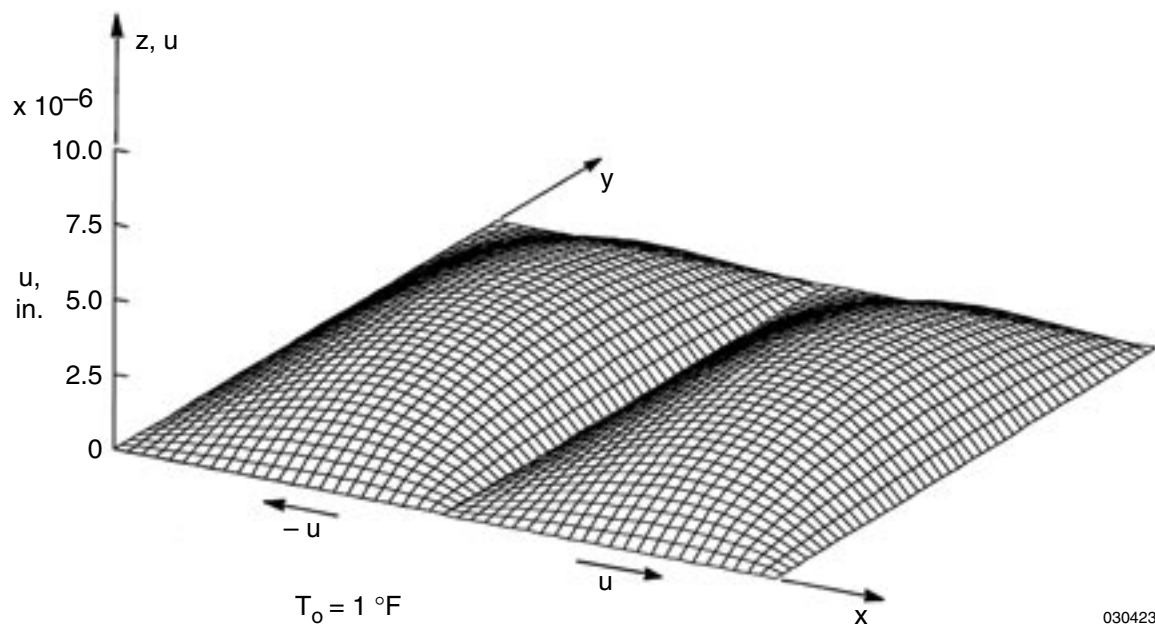


Figure 16. Distribution of x -displacement $u(x, y)$ in square panel ($a/b = 1$) under dome-shaped temperature profile heating; $T_o = 1$ °F; 4S fixed; $u(x, y) \neq 0$, $v(x, y) \neq 0$ at panel interior.

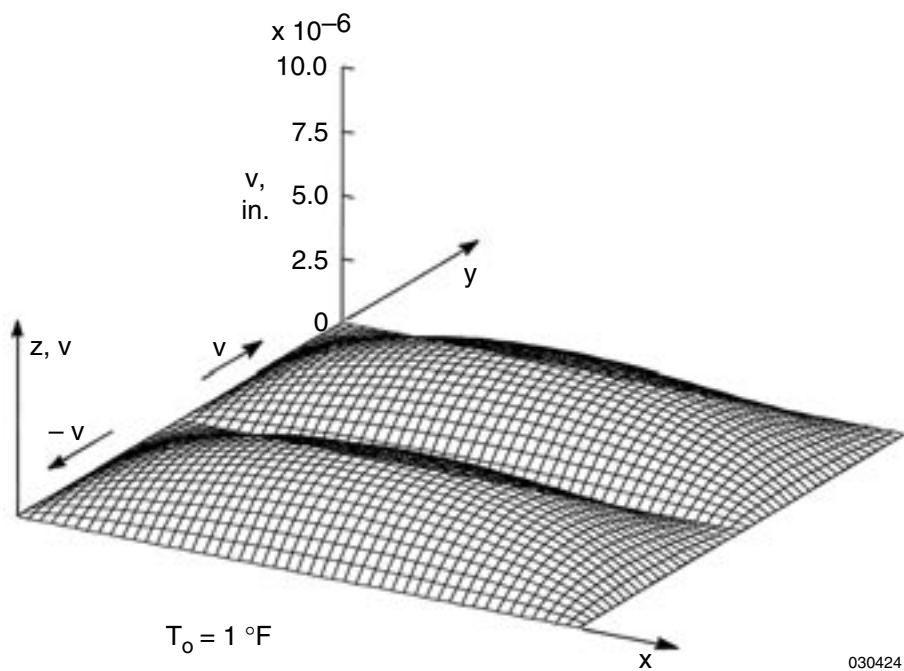


Figure 17. Distribution of y -displacement $v(x, y)$ in square panel ($a/b = 1$) under dome-shaped temperature profile heating; $T_o = 1$ °F; 4S fixed; $u(x, y) \neq 0$, $v(x, y) \neq 0$ at panel interior.

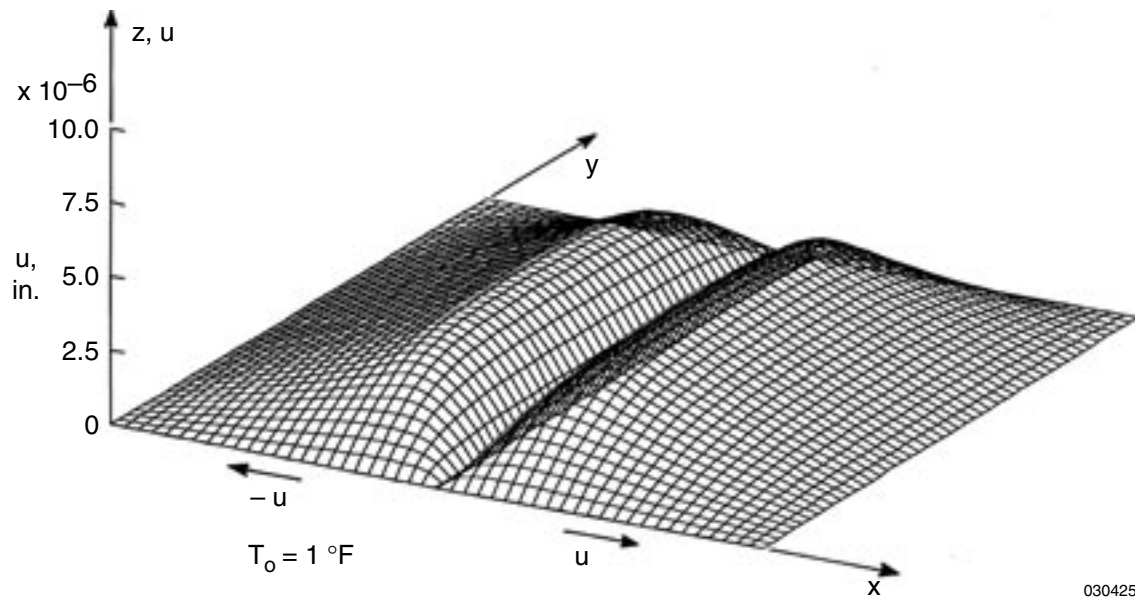


Figure 18. Distribution of x -displacement $u(x, y)$ in square panel ($a/b = 1$) under roof-shaped temperature profile heating; $T_o = 1 \text{ }^{\circ}\text{F}$; 4S fixed; $u(x, y) \neq 0, v(x, y) \neq 0$ at panel interior.

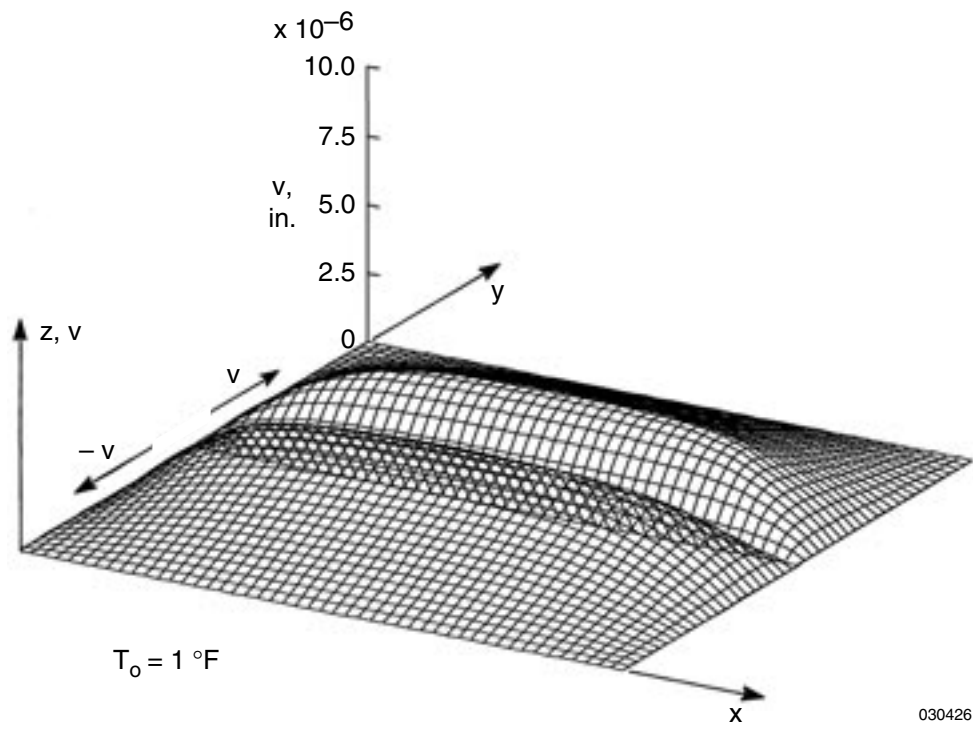


Figure 19. Distribution of y -displacement $v(x, y)$ in square panel ($a/b = 1$) under roof-shaped temperature profile heating; $T_o = 1 \text{ }^{\circ}\text{F}$; 4S fixed; $u(x, y) \neq 0, v(x, y) \neq 0$ at panel interior.

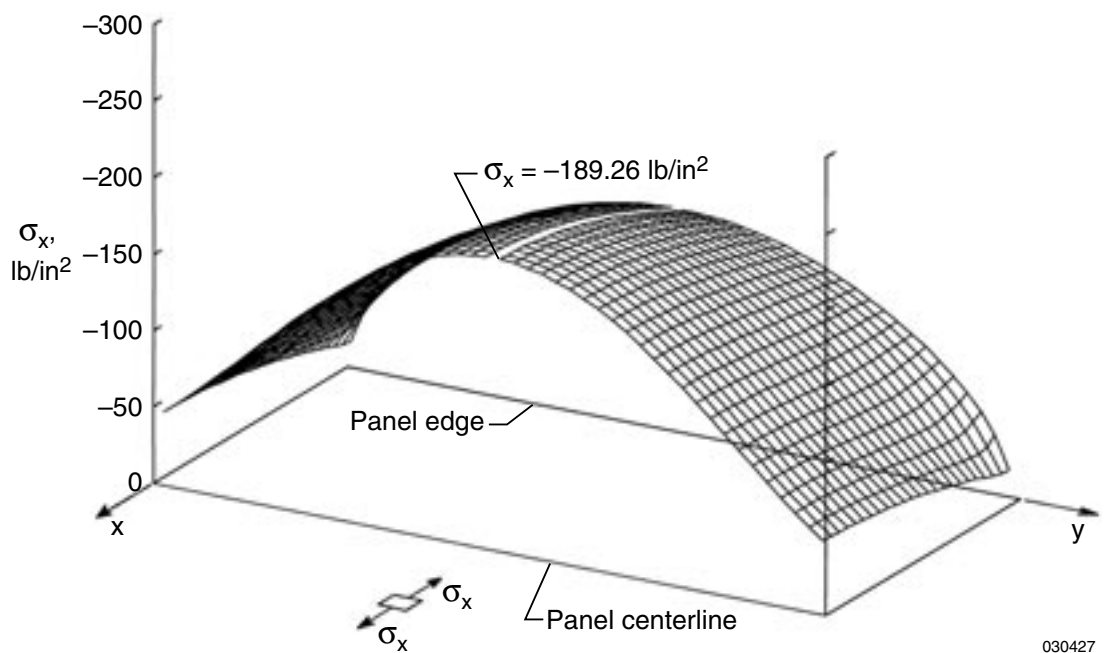


Figure 20. Distribution of $\sigma_x(x, y)$ in square panel ($a/b = 1$) under dome-shaped temperature profile heating; $T_o = 1$ °F; 4S fixed; $u(x, y) \neq 0$, $v(x, y) \neq 0$ at panel interior.

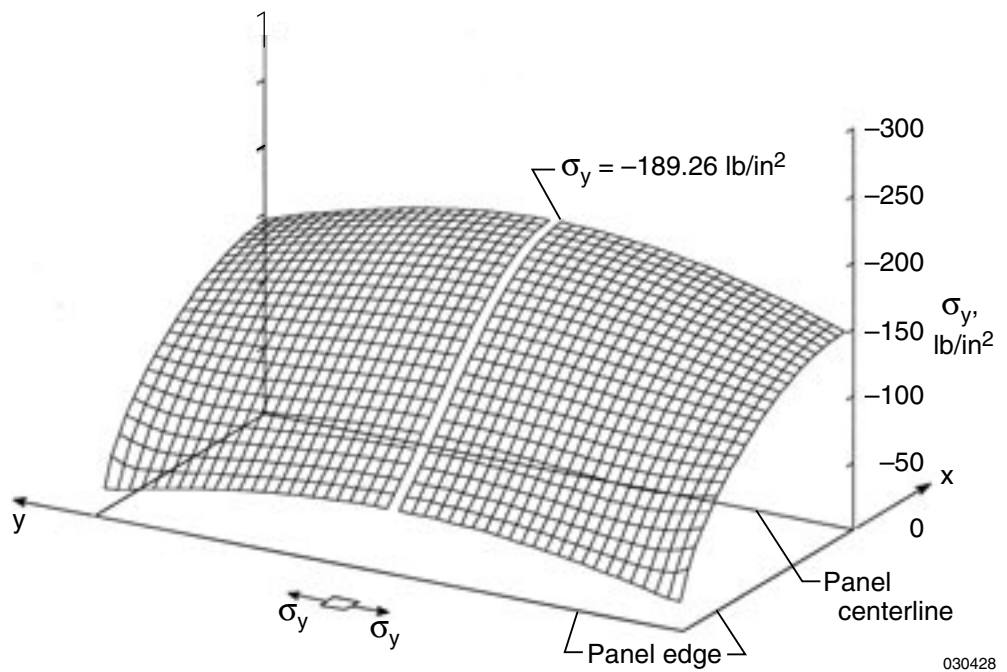


Figure 21. Distribution of $\sigma_y(x, y)$ in square panel ($a/b = 1$) under dome-shaped temperature profile heating; $T_o = 1$ °F; 4S fixed; $u(x, y) \neq 0$, $v(x, y) \neq 0$ at panel interior.

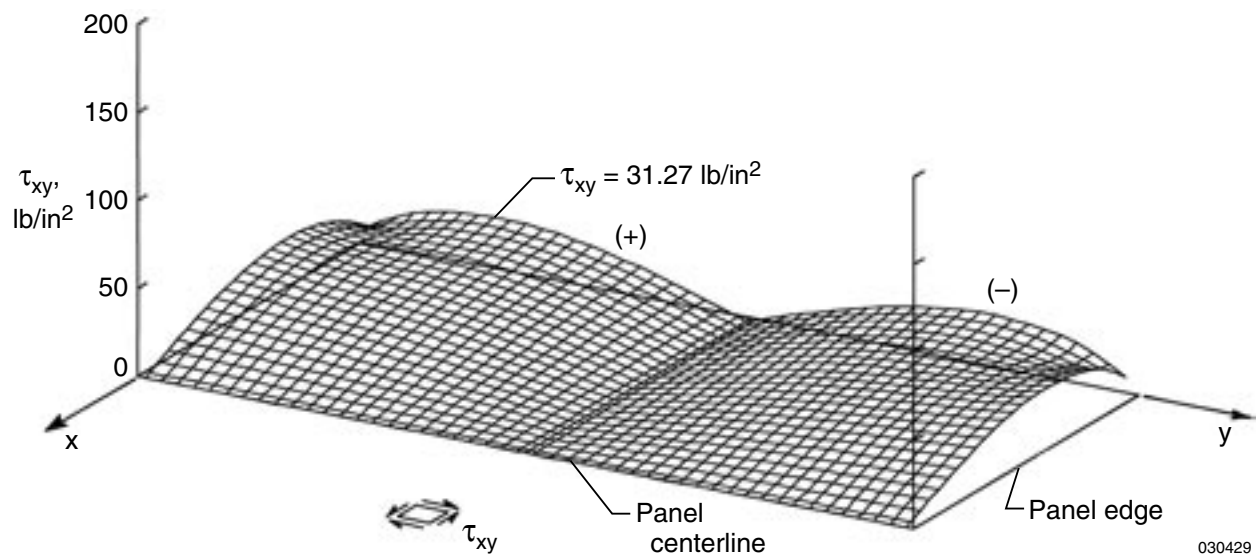


Figure 22. Distribution of $\tau_{xy}(x,y)$ in square panel ($a/b = 1$) under dome-shaped temperature profile heating; $T_o = 1$ °F; 4S fixed; $u(x,y) \neq 0$, $v(x,y) \neq 0$ at panel interior.

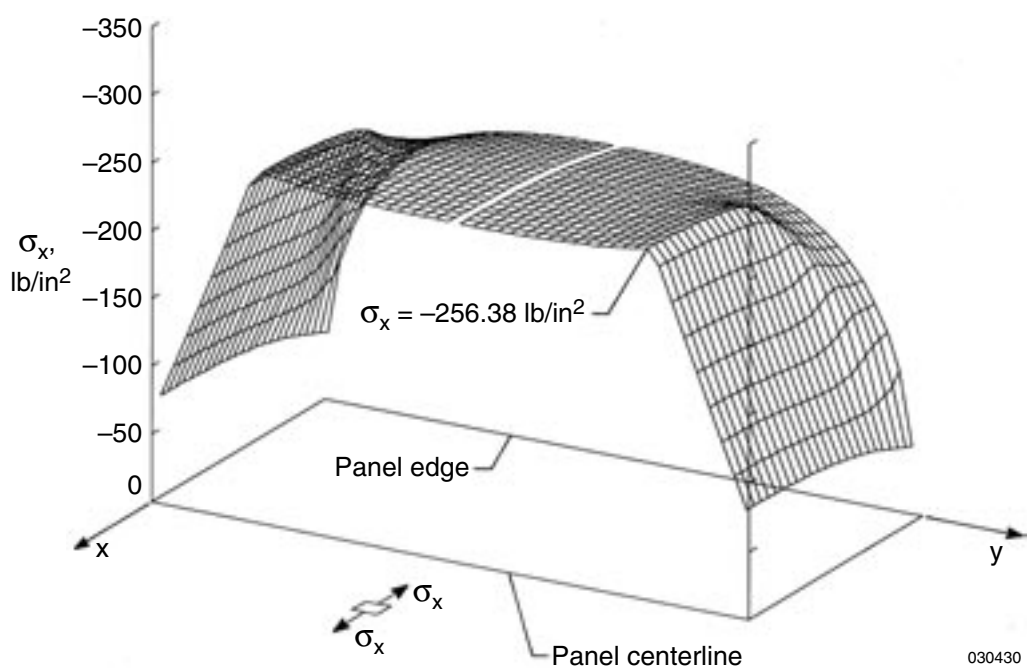


Figure 23. Distribution of $\sigma_x(x,y)$ in square panel ($a/b = 1$) under roof-shaped temperature profile heating; $T_o = 1$ °F; 4S fixed; $u(x,y) \neq 0$, $v(x,y) \neq 0$ at panel interior.

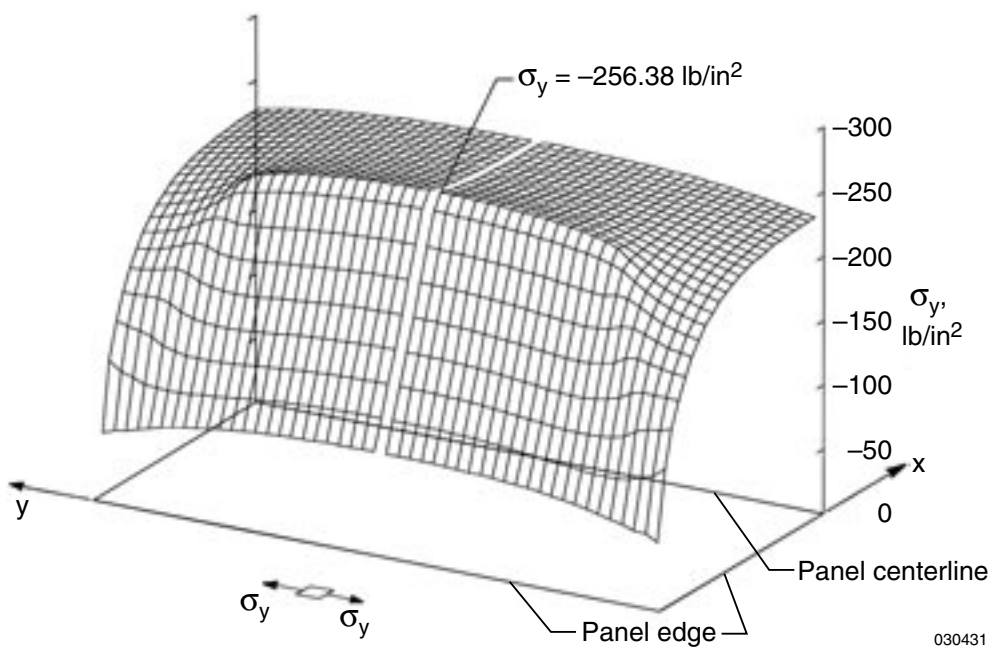


Figure 24. Distribution of $\sigma_y(x, y)$ in square panel ($a/b = 1$) under roof-shaped temperature profile heating; $T_o = 1$ °F; 4S fixed; $u(x, y) \neq 0, v(x, y) \neq 0$ at panel interior.

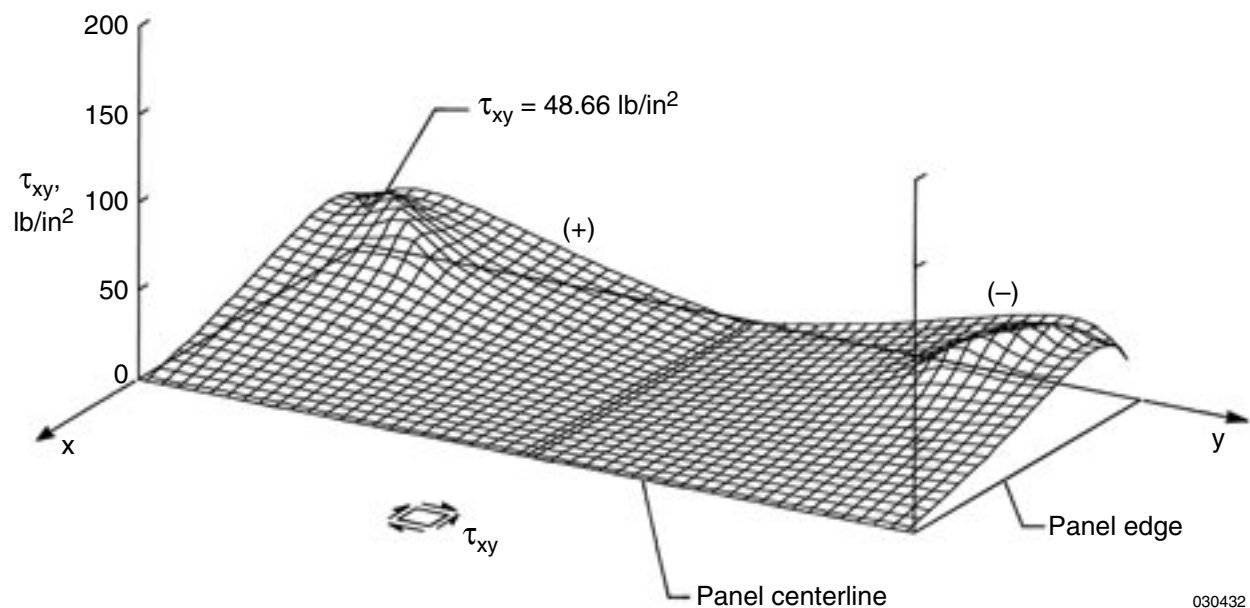


Figure 25. Distribution of $\tau_{xy}(x, y)$ in square panel ($a/b = 1$) under roof-shaped temperature profile heating; $T_o = 1$ °F; 4S fixed; $u(x, y) \neq 0, v(x, y) \neq 0$ at panel interior.

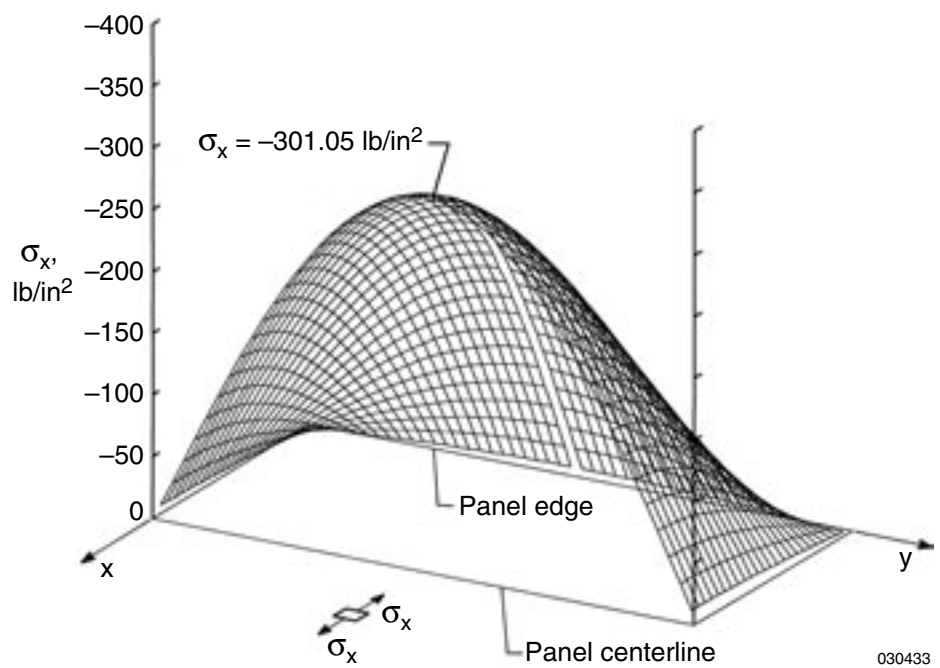


Figure 26. Distribution of $\sigma_x(x, y)$ in square panel ($a/b = 1$) under dome-shaped temperature profile heating; $T_o = 1$ °F; 4S fixed; $u(x, y) = v(x, y) = 0$ everywhere.

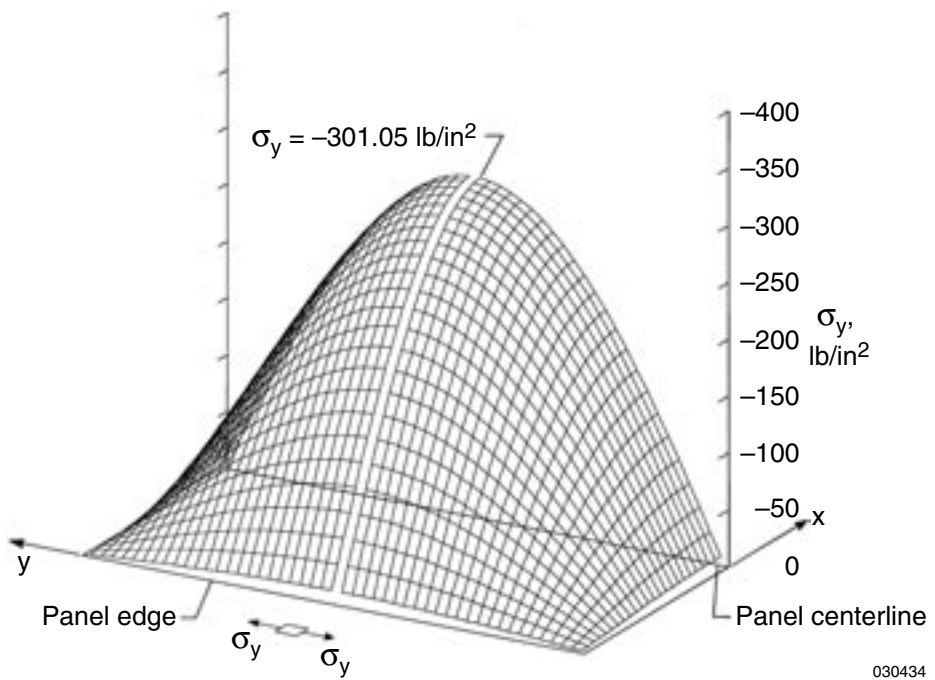


Figure 27. Distribution of $\sigma_y(x, y)$ in square panel ($a/b = 1$) under dome-shaped temperature profile heating; $T_o = 1$ °F; 4S fixed; $u(x, y) = v(x, y) = 0$ everywhere.

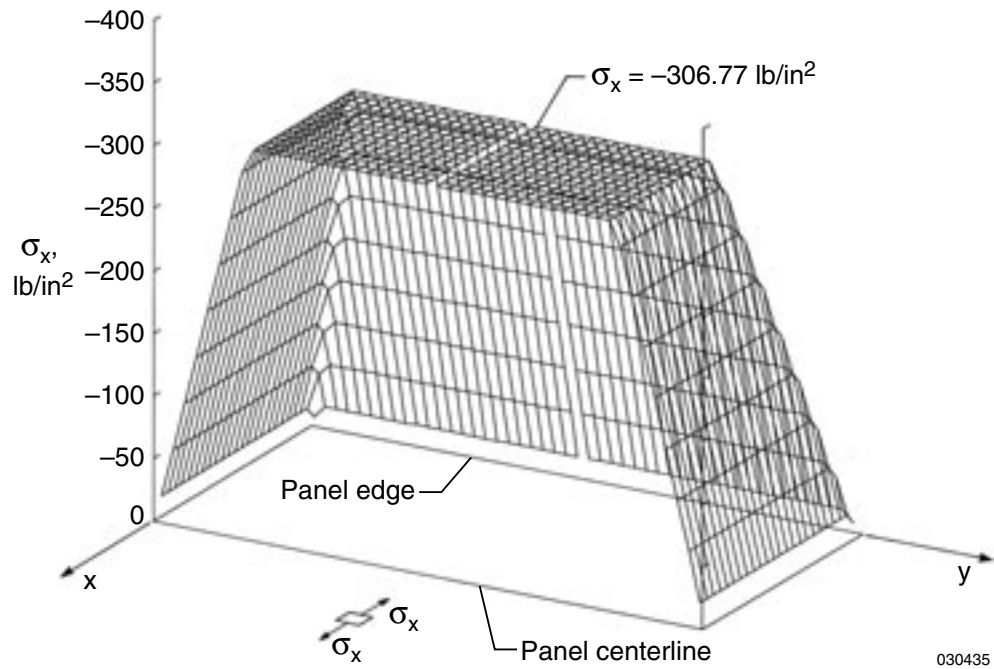


Figure 28. Distribution of $\sigma_x(x, y)$ in square panel ($a/b = 1$) under roof-shaped temperature profile heating; $T_o = 1^\circ\text{F}$; 4S fixed; $u(x, y) = v(x, y) = 0$ everywhere.

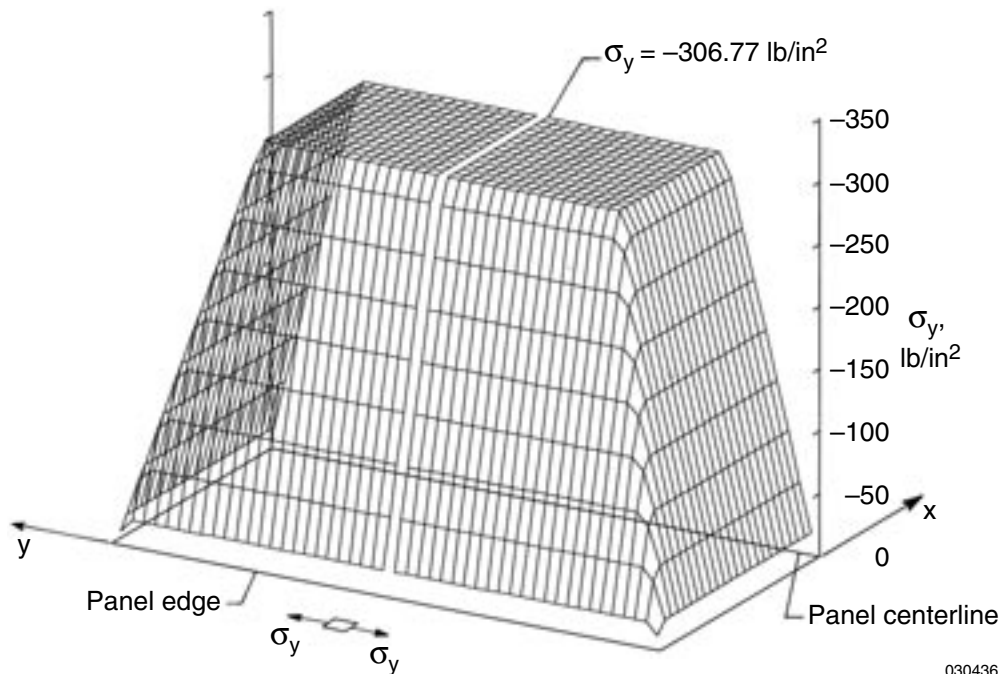


Figure 29. Distribution of $\sigma_y(x, y)$ in square panel ($a/b = 1$) under roof-shaped temperature profile heating; $T_o = 1^\circ\text{F}$; 4S fixed; $u(x, y) = v(x, y) = 0$ everywhere.

REPORT DOCUMENTATION PAGE			Form Approved OMB No. 0704-0188
<p>Public reporting burden for this collection of information is estimated to average 1 hour per response, including the time for reviewing instructions, searching existing data sources, gathering and maintaining the data needed, and completing and reviewing the collection of information. Send comments regarding this burden estimate or any other aspect of this collection of information, including suggestions for reducing this burden, to Washington Headquarters Services, Directorate for Information Operations and Reports, 1215 Jefferson Davis Highway, Suite 1204, Arlington, VA 22202-4302, and to the Office of Management and Budget, Paperwork Reduction Project (0704-0188), Washington, DC 20503.</p>			
1. AGENCY USE ONLY (Leave blank)	2. REPORT DATE	3. REPORT TYPE AND DATES COVERED	
	January 2004	Technical Publication	
4. TITLE AND SUBTITLE		5. FUNDING NUMBERS	
Thermal Buckling Analysis of Rectangular Panels Subjected to Humped Temperature Profile Heating		WU 090-50-00-SE-RR-00-000	
6. AUTHOR(S)			
William L. Ko			
7. PERFORMING ORGANIZATION NAME(S) AND ADDRESS(ES)		8. PERFORMING ORGANIZATION REPORT NUMBER	
NASA Dryden Flight Research Center P.O. Box 273 Edwards, California 93523-0273		H-2539	
9. SPONSORING/MONITORING AGENCY NAME(S) AND ADDRESS(ES)		10. SPONSORING/MONITORING AGENCY REPORT NUMBER	
National Aeronautics and Space Administration Washington, DC 20546-0001		NASA/TP-2004-212041	
11. SUPPLEMENTARY NOTES			
12a. DISTRIBUTION/AVAILABILITY STATEMENT		12b. DISTRIBUTION CODE	
Unclassified—Unlimited Subject Category 39			
This report is available at http://www.dfrc.nasa.gov/DTRS/			
13. ABSTRACT (Maximum 200 words)			
<p>This research investigates thermal buckling characteristics of rectangular panels subjected to different types of humped temperature profile heating. Minimum potential energy and finite-element methods are used to calculate the panel buckling temperatures. The two methods give fairly close thermal buckling solutions. “Buckling temperature magnification factor of the first kind, η” is established for the fixed panel edges to scale up the buckling solution of uniform temperature loading case to give the buckling solution of the humped temperature profile loading cases. Also, “buckling temperature magnification factor of the second kind, ξ” is established for the free panel edges to scale up the buckling solution of humped temperature profile loading cases with unheated boundary heat sinks to give the buckling solutions when the boundary heat sinks are heated up.</p>			
14. SUBJECT TERMS		15. NUMBER OF PAGES	
Buckling temperature magnification factors, Finite-element method, Humped temperature profile heating, Minimum potential energy method, Thermal buckling		56	
		16. PRICE CODE	
		A03	
17. SECURITY CLASSIFICATION OF REPORT	18. SECURITY CLASSIFICATION OF THIS PAGE	19. SECURITY CLASSIFICATION OF ABSTRACT	20. LIMITATION OF ABSTRACT
Unclassified	Unclassified	Unclassified	Unlimited